

Fig. 4. Product ion spectra of model oligosaccharide, TetraNA<sub>4</sub>. (A) MS<sup>2</sup> spectrum derived from [TetraNA<sub>4</sub>]<sup>3+</sup> at *m/z* 1180 in positive ion mode. (B) MS<sup>4</sup> spectrum derived from [TetraNA<sub>4</sub>]<sup>3-</sup> at *m/z* 1178 → [TetraNA<sub>3</sub>]<sup>3-</sup> at *m/z* 1081 → [TetraNA<sub>2</sub>]<sup>2-</sup> at *m/z* 1476 in negative ion mode.

with NaBH<sub>4</sub>. Fig. 5 shows total ion chromatogram (TIC) (A) obtained by GCC-LC/IT-MS-FT-ICR-MS of borohydrate-reduced oligosaccharides, and two-dimensional display of full MS<sup>1</sup> scans in positive ion mode (red) and negative ion mode (blue) (B), in which oligosaccharides appear as protonated and ammonium adducted forms along with fragment ions. Alternative scanning in positive and negative ion mode enables us to detect many oligosaccharides without missing less ionized oligosaccharides in either ion mode. For example, oligosaccharides at *m/z* 762 (2+) and 822 (2+) were detected only in positive ion mode, whereas those at *m/z* 1387 (2-), 1440 (2-), and 1542 (2-) were detected only in negative ion mode. Furthermore,

accurate *m/z* values acquired by FT-ICR-MS provide their monosaccharide composition, and subsequent data-dependent MS<sup>n</sup> allows us to elucidate their monosaccharide sequence as follows.

### 3.2.1. Monosaccharide composition of oligosaccharides

Oligosaccharides in Thy-1 were assigned to NeuAc<sub>0-3</sub>dHex<sub>0-3</sub>Hex<sub>3-9</sub>HexNAc<sub>1-5</sub>HexNAc<sub>ol1</sub> based on their accurate *m/z* values (Table 1). Oligosaccharides bearing two Fuc residues, in which the *m/z* values of multiple charged ions are nearly identical to those of oligosaccharides bearing one NeuAc residue instead, could be determined

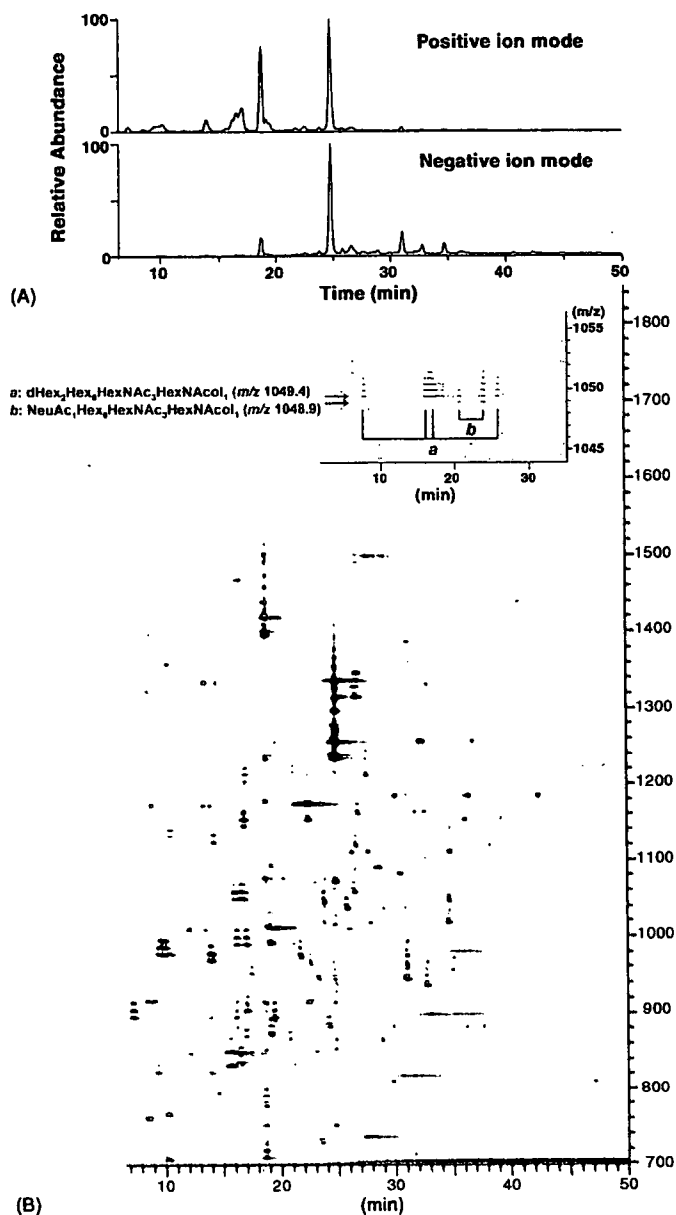


Fig. 5. N-Linked oligosaccharide profile of rat brain Thy-1 obtained by full MS<sup>1</sup> scans with FT-ICR-MS. (A) TIC, and (B) overlapped 2D display in positive (red) and negative (blue) ion modes.

by FT-ICR-MS. For instance, difucosylated oligosaccharides (dHex<sub>2</sub>Hex<sub>6</sub>HexNAC<sub>3</sub>HexNACol<sub>1</sub>, theoretical molecular weight: 2096.78 Da) detected at 7.6, 16, 17, and 26 min (Fig. 5, inset, a) were clearly distinguished from monosialylated oligosaccharides (NeuAc<sub>1</sub>Hex<sub>6</sub>HexNAC<sub>3</sub>HexNACol<sub>1</sub>, theoretical molecular weight: 2095.76 Da) detected at 21 and 24 min (Fig. 5, inset, b). The improved oligosaccharide profiling indicated that Thy-1 possesses a significant variety of N-linked oligosaccharides containing high-mannose-type (Man5, Man6, Man7, Man8, and M9) and many different complex- and hybrid-type oligosaccharides bearing NeuAc<sub>0-3</sub> and Fuc<sub>0-3</sub>. These results are coincident with those of our previous study, in which we carried out mass spectrometric analysis of Thy-1 glycopeptides.

### 3.2.2. Monosaccharide sequence of oligosaccharides

Monosaccharide sequences of oligosaccharides were elucidated based on the MS/MS spectra. One of the remarkable features of Thy-1 oligosaccharides is the attachment of multiple Fuc and NeuAc residues. We describe below some examples of assignment fucosylated and sialylated oligosaccharides.

**3.2.2.1. Gal-(Fuc-)-GlcNAc-(Lewis a/x type).** Fig. 6A shows the product ion spectrum of a difucosylated oligosaccharide, dHex<sub>2</sub>Hex<sub>4</sub>HexNAC<sub>3</sub>HexNACol<sub>1</sub>, at *m/z* 887 (24.3 min) in positive ion mode. There are two possible sites of fucosylation: GlcNAc at the non-reducing end and at the reducing end in the trimannosyl core. The ions detected at *m/z* 350 (Fuc-GlcNAc<sup>+</sup>, B<sub>2α</sub>/Y<sub>5α'</sub><sup>+</sup>), 370 (Fuc-GlcNAcol<sup>+</sup>, Y<sub>1α</sub><sup>+</sup>), and 512 (Gal-(Fuc-)-GlcNAc<sup>+</sup>, B<sub>2α</sub><sup>+</sup>) indicate that Fuc residues link to both the non-reducing end like Lewis a/x, and the inner trimannosyl core GlcNAc. Other ions detected at *m/z* 1553 (Z<sub>3γ</sub><sup>+</sup>, [Y<sub>3γ</sub>-H<sub>2</sub>O]<sup>+</sup>) and 1570 (Y<sub>3γ</sub><sup>+</sup>) suggest a linkage of non-substituted HexNac at the terminal end. From these characteristic ions together with a Y ion at *m/z* 938.03 (Y<sub>3α/3β</sub><sup>+</sup>), it can be deduced that this HexNac is a bisecting GlcNAc that attaches to the core mannose residue via β1-4 linkage. On the basis of these product ions, the oligosaccharide is assigned to the structure indicated in Fig. 6A, inset.

**3.2.2.2. Fuc-Gal-(Fuc-)-GlcNAc-(Lewis b/y type).** Fig. 6B is the product ion spectrum of a difucosylated oligosaccharide, dHex<sub>2</sub>Hex<sub>5</sub>HexNAC<sub>4</sub>HexNACol<sub>1</sub>, at *m/z* 1070 (9.2 min). The characteristic ions at *m/z* 512 (Gal-(Fuc-)-GlcNAc<sup>+</sup>, Fuc-Gal-GlcNAc<sup>+</sup>, B<sub>3α</sub>/Y<sub>6α'''</sub><sup>+</sup>, B<sub>3α</sub>/Y<sub>5α'''</sub><sup>+</sup>) and 1915 (B<sub>6</sub><sup>+</sup>) suggest the absence of Fuc at the reducing end GlcNAc; a B ion at *m/z* 658 (B<sub>3α</sub><sup>+</sup>), a B/Y ion at *m/z* 350, and a Y ion at *m/z* 1408 (Y<sub>3β/4α''</sub><sup>+</sup>) suggest the attachment of two Fuc to Gal-GlcNAc at the non-reducing end, in a similar manner to the Lewis b/y antigen, Fuc-Gal-(Fuc-)-GlcNAc-. A Y ion at *m/z* 1936 (Y<sub>4α''</sub><sup>+</sup>) indicates a linkage of non-substituted HexNac at the terminal end. A B/Y ion at *m/z* 877 (B<sub>4α</sub>/Y<sub>5α'''</sub><sup>+</sup>, B<sub>4α</sub>/Y<sub>6α'''</sub><sup>+</sup>) and a Y ion at *m/z* 1610 (Y<sub>3β</sub><sup>+</sup>) suggest that this non-substituted HexNac residue is linked to the mannose residue attached to the Fuc-Gal-(Fuc-)-GlcNAc- structure. These ions lead to assignment of this oligosaccharide as the structure indicated in Fig. 6B, inset.

**3.2.2.3. NeuAc-Gal-(NeuAc-)-GlcNAc-.** Fig. 7A shows the product ion spectrum of a disialylated oligosaccharide, NeuAc<sub>2</sub>dHex<sub>1</sub>Hex<sub>5</sub>HexNAC<sub>2</sub>HexNACol<sub>1</sub>, at *m/z* 1085 (30.4 min). Characteristic fragment ions at *m/z* 495 (B<sub>3α</sub>/Y<sub>5α'</sub><sup>+</sup>), 948 (B<sub>3α</sub><sup>+</sup>), and 1110 (B<sub>4α</sub><sup>+</sup>), together with B ions at *m/z* 453 (B<sub>2α</sub><sup>+</sup>) and 657 (B<sub>3α</sub>/Y<sub>5α''</sub><sup>+</sup>, B<sub>3α</sub>/Y<sub>6α''</sub><sup>+</sup>) suggest the presence of a partial structure of NeuAc-Gal-(NeuAc-)-GlcNAc-. Furthermore, detection of Y ions at *m/z* 370 (Y<sub>1α</sub><sup>+</sup>) and 1059 (Y<sub>3α</sub><sup>+</sup>, Y<sub>4α/4β</sub><sup>+</sup>) as well as a B ion at *m/z* 1799 (B<sub>6</sub><sup>+</sup>) indicate the linkage of a Fuc residue at the inner trimannosyl core GlcNAc. Based on these product ions, the oligosaccharide detected at *m/z* 1085 was assigned to the structure in Fig. 7A, inset.

Table 1  
Summary of N-linked oligosaccharides of rat brain Thy-1

Monosaccharidic composition <sup>a</sup>				Theoretical mass <sup>b</sup>	Positive ion mode		Negative ion mode		Deduced structure <sup>d</sup>
dHex	Hex	HX	NA		Observed m/z <sup>c</sup>	Retention time (min)	Observed m/z <sup>c</sup>	Retention time (min)	
1	3	2	0	1058.40	1059.46(1)	29.17			CoreF
0	5	2	0	1236.45	1237.47(1)	24.74	1235.45(1)	24.76	M5
0	3	4	0	1318.50	1319.57(1)	8.63			
0	6	2	0	1398.50	1399.53(1)	18.73	1397.50(1)	18.68	M6
0	5	3	0	1439.53	1440.59(1)	9.17			
1	3	4	0	1464.56	733.31(2), 1465.65(1)	23.44			
0	3	5	0	1521.58	761.80(2)	8.63			BisectGN
0	7	2	0	1560.55	781.29(2), 1561.60(1)	18.66			M7
1	5	3	0	1585.59	793.82(2)	14.59			Hybrid
1	5	3	0	1585.59	793.81(2)	19.13			
1	5	3	0	1585.59	793.83(2)	20.96			
0	5	4	0	1642.61	822.33(2)	9.48			Hybrid
0	5	4	0	1642.61	822.33(2)	14.02			
1	3	5	0	1667.64	834.83(2), 1668.69(1)	16.48	832.81(2)	16.44	CoreF
0	4	5	0	1683.63	842.85(2)	17.48			Hybrid
0	8	2	0	1722.61	870.83(2) <sup>e</sup>	17.07			M8
0	5	3	1	1730.62	866.34(2)	20.31			
0	5	3	1	1730.62	866.35(2)	28.91	864.31(2), 1729.64(1)	28.93	Hybrid
2	5	3	0	1731.64	866.86(2)	20.83	864.81(2)	20.85	Hybrid, CoreF, Lax
1	6	3	0	1747.64	874.84(2)	19.19			
2	4	4	0	1772.67	887.37(2)	23.84	885.33(2)	23.86	
2	4	4	0	1772.67	887.36(2)	24.25	885.33(2)	24.27	Hybrid, CoreF, BisectGN
1	5	4	0	1788.67	895.36(2)	7.37			Hybrid
1	5	4	0	1788.67	895.36(2)	13.90			
1	5	4	0	1788.67	895.35(2)	14.16			Hybrid, CoreF
1	5	4	0	1788.67	895.35(2)	19.44	893.33(2)	19.46	Hybrid, CoreF
0	6	4	0	1804.66	903.35(2)	17.07	901.33(2)	17.09	Hybrid, BisectGN
1	4	5	0	1829.69	915.88(2)	8.63			Hybrid
1	4	5	0	1829.69	915.88(2)	9.17			Hybrid
1	4	5	0	1829.69	915.89(2)	18.00			Hybrid
1	4	5	0	1829.69	915.89(2)	22.61	913.84(2)	22.63	
1	5	3	1	1876.68	939.37(2)	21.17	937.34(2)	21.12	
1	5	3	1	1876.68	939.36(2)	24.90	937.34(2)	24.92	
1	5	3	1	1876.68	939.39(2)	32.76	937.33(2)	32.78	Hybrid, CoreF
0	9	2	0	1884.66	951.88(2) <sup>e</sup>	17.53			M9
0	6	3	1	1892.68	947.39(2)	23.31	945.33(2)	23.33	Hybrid
0	6	3	1	1892.68	947.39(2)	31.09	945.33(2)	31.05	Hybrid
2	6	3	0	1893.70	947.87(2)	24.61	945.84(2)	24.70	
1	4	4	1	1917.71			957.85(2)	27.73	
1	4	4	1	1917.71			957.85(2)	28.86	
1	4	4	1	1917.71			957.85(2)	34.91	CoreF
1	4	4	1	1917.71			957.85(2)	35.55	
0	5	4	1	1933.70	967.89(2)	22.61	965.85(2)	22.63	Hybrid
0	5	4	1	1933.70	967.86(2)	24.61	965.82(2)	24.70	
2	5	4	0	1934.72	968.39(2)	13.97			Hybrid
1	6	4	0	1950.72	976.39(2)	9.93			Hybrid, Lax
1	6	4	0	1950.72	976.41(2)	21.76	974.35(2)	21.79	Hybrid, CoreF
2	4	5	0	1975.75	988.90(2)	16.21	986.85(2)	16.16	Complex
2	4	5	0	1975.75	988.90(2)	17.07	986.87(2)	17.09	Complex
0	5	3	2	2021.72			1009.86(2)	26.35	
0	5	3	2	2021.72			1009.85(2)	26.83	
1	6	3	1	2038.73	1020.40(2)	23.84	1018.36(2)	23.80	
1	6	3	1	2038.73	1020.44(2)	27.77	1018.37(2)	27.80	CoreF
1	6	3	1	2038.73	1020.42(2)	34.66	1018.36(2)	34.69	Hybrid, CoreF
1	5	4	1	2079.76	1040.92(2)	25.73	1038.87(2)	25.81	CoreF
1	5	4	1	2079.76	1040.92(2)	29.04	1038.88(2)	28.99	
3	5	4	0	2080.78	1041.42(2)	23.84	1039.39(2)	23.86	
0	6	4	1	2095.76	1048.94(2)	20.57			Hybrid
0	6	4	1	2095.76	1048.91(2)	23.84	1046.87(2)	23.80	Hybrid
2	6	4	0	2096.78	1049.42(2)	7.58			

Table 1 (Continued)

Monosaccharide composition <sup>a</sup>				Theoretical mass <sup>b</sup>	Positive ion mode		Negative ion mode		Deduced structure <sup>d</sup>
dHex	Hex	HX	NA		Observed <i>m/z</i> <sup>c</sup>	Retention time (min)	Observed <i>m/z</i> <sup>c</sup>	Retention time (min)	
2	6	4	0	2096.78	1049.42(2)	15.97			
2	6	4	0	2096.78	1049.42(2)	16.61			Hybrid, BisectGN
2	6	4	0	2096.78	1049.43(2)	25.73			
1	7	4	0	2112.77			1055.38(2)	34.62	
1	4	5	1	2120.79	1061.45(2)	20.43			Complex
1	4	5	1	2120.79	1061.45(2)	24.74	1059.39(2)	24.70	
1	4	5	1	2120.79	1061.45(2)	26.47	1059.39(2)	26.42	CoreF
2	5	5	0	2137.80	1069.94(2)	9.17			Lby
2	5	5	0	2137.80	1069.94(2)	21.30			
2	5	5	0	2137.80	1069.95(2)	23.09	1067.9(2)	23.04	
1	5	3	2	2167.78	1084.94(2)	30.41	1082.89(2)	30.37	Hybrid, CoreF
2	4	6	0	2178.83	1090.45(2)	26.08			
0	6	3	2	2183.77	1092.95(2)	28.63	1090.88(2)	28.60	Hybrid, diSia
0	5	4	2	2224.80	1113.45(2)	26.10			
2	5	4	1	2225.82	1113.95(2)	27.56			
2	5	4	1	2225.82	1113.98(2)	34.80			
1	6	4	1	2241.81	1121.95(2)	26.60	1119.90(2)	26.63	
1	6	4	1	2241.81			1119.90(2)	30.58	
1	6	4	1	2241.81			1119.91(2)	38.14	
3	6	4	0	2242.83	1122.46(2)	14.23			
2	7	4	0	2258.83	1130.46(2)	10.47			
3	5	5	0	2283.86	1142.96(2)	16.87			
1	4	6	1	2323.87	1162.98(2)	26.60			
1	6	3	2	2329.83			1163.91(2)	31.72	
1	6	3	2	2329.83			1163.91(2)	32.54	Hybrid, diSia
1	5	4	2	2370.86	1186.55(2)	29.89	1184.42(2)	30.00	Complex, CoreF
1	5	4	2	2370.86			1184.43(2)	36.00	
1	5	4	2	2370.86	1186.52(2)	36.31	1184.42(2)	36.40	Complex, CoreF
1	5	4	2	2370.86	1186.50(2)	42.47	1184.43(2)	42.43	Complex, CoreF
3	5	4	1	2370.86			1184.93(2)	30.99	
2	5	5	1	2428.90	1215.50(2)	21.17	1213.44(2)	21.25	
2	5	5	1	2428.90	1215.50(2)	23.84			
2	5	5	1	2428.90	1215.52(2)	26.32	1213.45(2)	26.28	
2	5	5	1	2428.90	1215.50(2)	27.50	1213.45(2)	27.53	
2	5	4	2	2516.91	1259.60(2)	32.23	1257.45(2)	32.19	Complex, Lax, CoreF, diSia
2	5	4	2	2516.91			1257.45(2)	36.72	
2	5	6	1	2631.98			876.32(3), 1314.99(2)	26.76	
3	5	4	2	2662.97			1330.49(2)	32.78	
1	5	6	2	2777.02			1387.50(2)	30.99	
0	6	5	3	2881.03			1439.50(2)	34.83	
0	6	5	3	2881.03			1439.49(2)	40.77	
2	6	5	2	2882.05			1440.05(2)	37.96	
2	6	6	2	3085.13			1541.55(2)	31.38	

<sup>a</sup> dHex, deoxyhexose; Hex, hexose; HX, *N*-acetylhexamine; NeuAc, *N*-acetylneuramic acid.

<sup>b</sup> Monoisotopic value.

<sup>c</sup> Values in parentheses are charge state.

<sup>d</sup> Structures are deduced by MS<sup>n</sup>. Complex, complex-type-oligosaccharide; Hybrid, hybrid-type-oligosaccharide; M5-9, high-mannose-type oligosaccharide containing 5–9 mannose residues; BisectGN, bisecting GlcNAc; Lax, Lewis a/x structure; Lby, Lewis b/y structure; diSia, disialic acid.

<sup>e</sup> Ammonium adducted form.

3.2.2.4. *NeuAc-Gal-GlcNAc*-. Fig. 7B shows the product ion spectrum of a disialylated oligosaccharide, NeuAc<sub>2</sub>dHex<sub>1</sub>Hex<sub>5</sub>HexNAc<sub>3</sub>HexNAcol<sub>1</sub>, at *m/z* 1187 (42.5 min). Although B ions were detected at *m/z* 454 (B<sub>2x</sub><sup>+</sup>), 657 (B<sub>3x</sub><sup>+</sup>) and 819 (B<sub>4x</sub><sup>+</sup>), none of the fragment ions at *m/z* 495 (NeuAc-GlcNAc<sup>+</sup>), 948 (NeuAc-Gal-(NeuAc-)GlcNAc<sup>+</sup>), or 1110 (NeuAc-Gal-(NeuAc-)GlcNAc-Man<sup>+</sup>) were detected in the spectrum. This result suggests that the two NeuAc residues occupy both non-reducing ends of the biantennary

form. Fucosylation of the inner trimannosyl core GlcNAc was determined by the detection of Y ions at *m/z* 370 (Y<sub>1a</sub><sup>+</sup>) and 1059 (Y<sub>4a/4b</sub><sup>+</sup>). These product ions lead to assignment of this oligosaccharide the structure in Fig. 6B.

3.2.2.5. (*v*) *NeuAc-NeuAc*-. Fig. 7C shows the product ion spectrum of a disialylated and difucosylated oligosaccharide, NeuAc<sub>2</sub>dHex<sub>2</sub>Hex<sub>5</sub>HexNAc<sub>3</sub>HexNAcol<sub>1</sub>, at *m/z* 1260 (32.2 min). The characteristic ions at *m/z* 583 (NeuAc-NeuAc<sup>+</sup>,

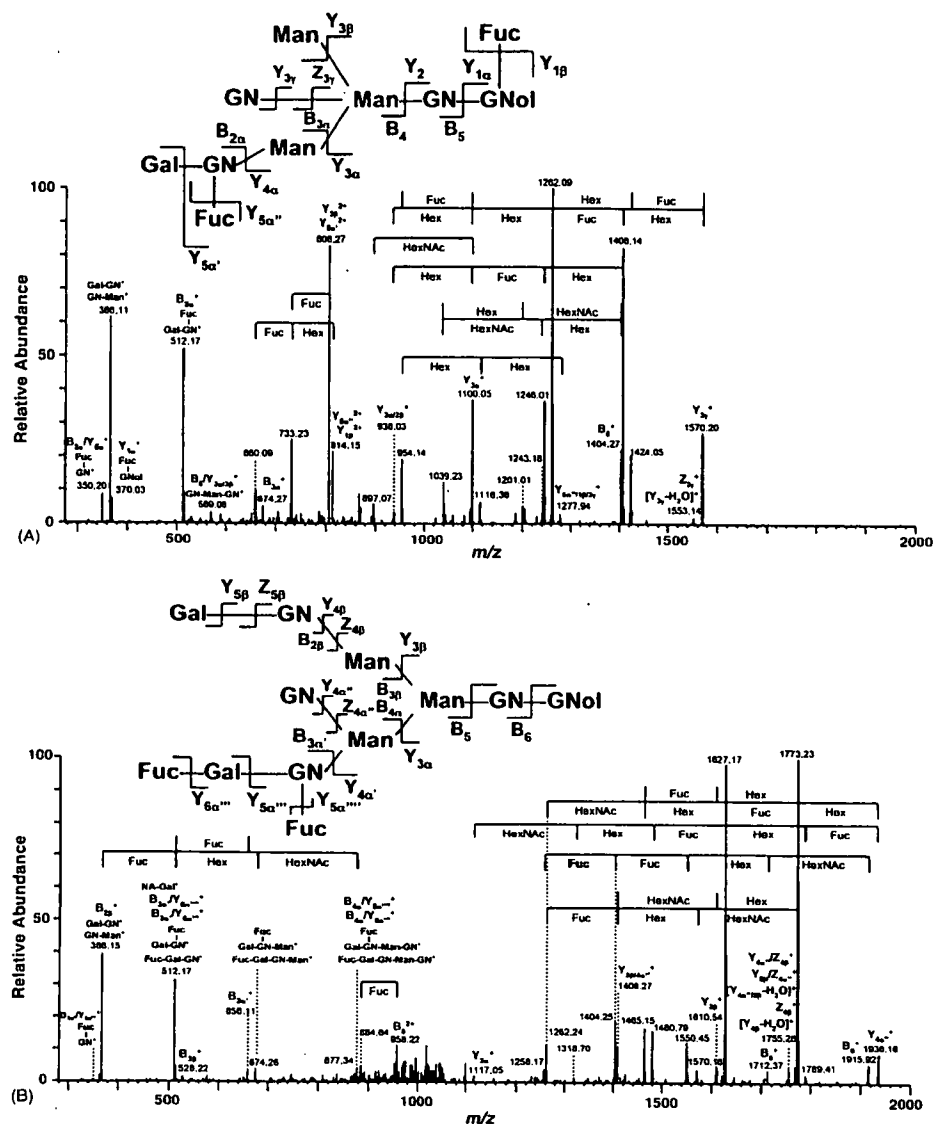


Fig. 6. Product ion spectra of N-linked oligosaccharides of rat brain Thy-1. (A) MS<sup>2</sup> spectrum of dHex<sub>2</sub>Hex<sub>4</sub>HexNAc<sub>3</sub>HexNAcol<sub>1</sub> at *m/z* 887 (24.3 min). (B) MS<sup>2</sup> spectrum of dHex<sub>2</sub>Hex<sub>5</sub>HexNAc<sub>4</sub>HexNAcol<sub>1</sub> at *m/z* 1070 (9.2 min).

B<sub>2α</sub><sup>+</sup>, 949 (NeuAc-NeuAc-Gal-GlcNAc<sup>+</sup>, B<sub>3α</sub>/Y<sub>5α</sub><sup>+</sup>), and 1094 (NeuAc-NeuAc-Gal-(Fuc-)GlcNAc<sup>+</sup>, B<sub>3α</sub><sup>+</sup>) suggest that this oligosaccharide contains a disialic acid residue and one Fuc at the non-reducing end. In addition, a Y ion at *m/z* 370 (Y<sub>1α</sub><sup>+</sup>) indicated that the other Fuc was attached to GlcNAc at the reducing end. Based on these product ions, this oligosaccharide structure could be assigned as indicated in Fig. 7C, inset.

#### 4. Discussion

Thy-1 has three N-glycosylation sites, Asn23, 74, and 98. We have previously demonstrated the attachment of high-mannose-type, complex-type, and hybrid-type oligosaccharides to these sites. Asn74 is occupied with various N-glycans, which have

been estimated to be fucosylated and sialylated [31]. Product ion spectra containing fucosylation and sialylation isomers make it difficult to elucidate the detailed structure. We have conducted mass spectrometric oligosaccharide analysis through the separation of diverse oligosaccharides with GCC. We first improved the mass spectrometric oligosaccharide profiling by IT-MS-FT-ICR-MS. The improved method enabled the monosaccharide composition analysis and sequencing of both neutral and acidic oligosaccharides in a single run. Using this method, we successfully analyzed various N-glycans of Thy-1 that could not be characterized by the analysis of glycopeptides. We found a Lewis b/y structure and sialylated GlcNAc in the branch structure. Interestingly, disialic acid (NeuAc-NeuAc-), which is known to be involved in neurite formation was found in brain Thy-1 [38].

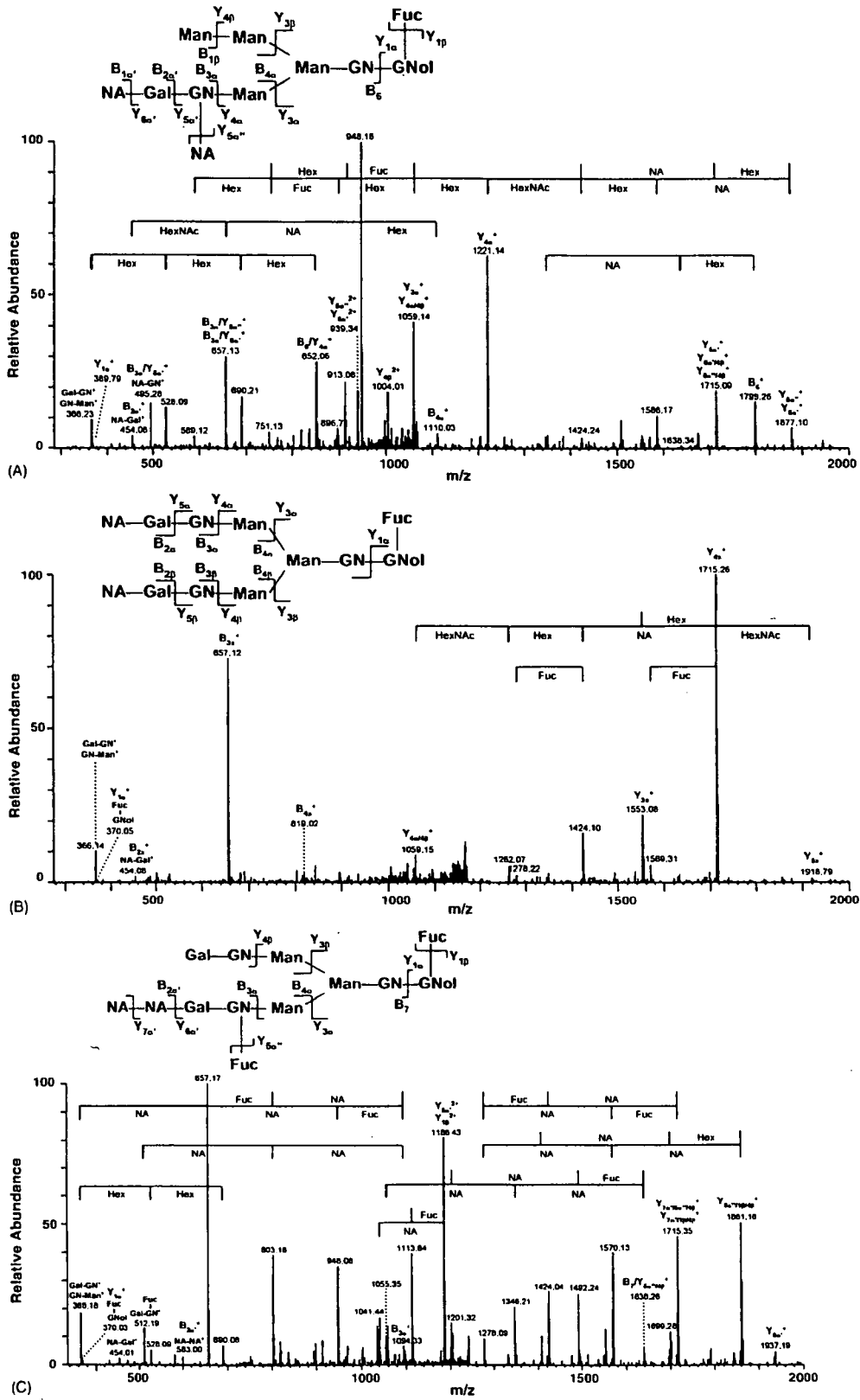


Fig. 7. Product ion spectra of N-linked oligosaccharides of rat brain Thy-1. (A) MS<sup>2</sup> spectrum of NeuAc<sub>2</sub>dHex<sub>1</sub>Hex<sub>5</sub>HexNAc<sub>2</sub>HexNAcol<sub>1</sub> at m/z 1085 (30.4 min). (B) MS<sup>2</sup> spectrum of NeuAc<sub>2</sub>dHex<sub>1</sub>Hex<sub>3</sub>HexNAc<sub>3</sub>HexNAcol<sub>1</sub> at m/z 1187 (42.5 min). (C) MS<sup>2</sup> spectrum of NeuAc<sub>2</sub>dHex<sub>2</sub>Hex<sub>5</sub>HexNAc<sub>3</sub>HexNAcol<sub>1</sub> at m/z 1260 (32.2 min).

In these two studies, we have demonstrated a strategy for glycosylation analysis of Thy-1, including identification of a glycoprotein, determination of glycosylation sites, site-specific glycosylation analysis, and structural analysis of oligosaccharide details. This strategy can be applied to glycosylation analysis of other glycoproteins. Specifically, the glycoprotein sample is divided into two. One is subjected to proteinase digestion followed by peptide/glycopeptide mapping, which provides information on glycosylation sites and site-specific heterogeneity. The other is subjected to PNGase F digestion followed by mass spectrometric oligosaccharide profiling, by which a detailed structure of *N*-glycans released from a glycoprotein could be provided. Recently, proteomic approaches, which are based on two-dimensional electrophoresis followed by mass spectrometry, have been used in various fields. Although glycosylation analysis of abundant glycoproteins in gel has been successful, that of a low-abundance glycoprotein in gel remains a great challenge. The proposed method consisting of peptide/glycopeptide mapping followed by oligosaccharide profiling with sequential scans by IT-MS-FT-ICR-MS will likely be a powerful tool for glycosylation analysis of low-abundance glycoproteins and for proteomics/glycomics.

#### Acknowledgements

This work was supported in part by a Grant-in-Aid for Creative Scientific Research (16GS0313) from the Ministry of Education, Culture, Sports, and Technology, the Ministry of Health, Labor and Welfare, and Core Research for the Evolutional Science and Technology Program (CREST) of the Japan Science and Technology Agency (JST).

We appreciate Dr. A. Hachisuka of the National Institute of Health Science for her technical advice.

We thank Dr. M. Kubota and Mr. M. Yoshida of Thermo Electron K.K. (Japan) for their technical support.

#### References

- [1] A. Varki, *Glycobiology* 3 (1993) 97.
- [2] J.W. Dennis, M. Granovsky, C.E. Warren, *Biochim. Biophys. Acta* 1473 (1999) 21.
- [3] Y. Sato, M. Kimura, C. Yasuda, Y. Nakano, M. Tomita, A. Kobata, T. Endo, *Glycobiology* 9 (1999) 655.
- [4] G. Durand, N. Seta, *Clin. Chem.* 46 (2000) 795.
- [5] O. Krokhin, W. Ens, K.G. Standing, J. Wilkins, H. Perreault, *Rapid Commun. Mass Spectrom.* 18 (2004) 2020.
- [6] Y. Satomi, Y. Shimonishi, T. Takao, *FEBS Lett.* 576 (2004) 51.
- [7] Y. Wada, M. Tajiri, S. Yoshida, *Anal. Chem.* 76 (2004) 6560.
- [8] W. Chai, V. Piskarev, A.M. Lawson, *Anal. Chem.* 73 (2001) 651.
- [9] D. Sagi, J. Peter-Katalinic, H.S. Conrad, M. Nimtz, *J. Am. Soc. Mass Spectrom.* 13 (2002) 1138.
- [10] A. Zamfir, D.G. Seidler, H. Kresse, J. Peter-Katalinic, *Glycobiology* 13 (2003) 733.
- [11] D.J. Harvey, R.L. Martin, K.A. Jackson, C.W. Sutton, *Rapid Commun. Mass Spectrom.* 18 (2004) 2997.
- [12] C. Robbe, C. Capon, B. Coddeville, J.C. Michalski, *Rapid Commun. Mass Spectrom.* 18 (2004) 412.
- [13] N. Ojima, K. Masuda, K. Tanaka, O. Nishimura, *J. Mass Spectrom.* 40 (2005) 380.
- [14] C.W. Sutton, J.A. O'Neill, J.S. Cottrell, *Anal. Biochem.* 218 (1994) 34.
- [15] B. Küster, S.F. Wheeler, A.P. Hunter, R.A. Dwek, D.J. Harvey, *Anal. Biochem.* 250 (1997) 82.
- [16] B. Küster, T.N. Krogh, E. Mortz, D.J. Harvey, *Proteomics* 1 (2001) 350.
- [17] K. Hirayama, R. Yuji, N. Yamada, K. Kato, Y. Arata, I. Shimada, *Anal. Chem.* 70 (1998) 2718.
- [18] F. Wang, A. Nakouzi, R.H. Angeletti, A. Casadevall, *Anal. Biochem.* 314 (2003) 266.
- [19] K. Sandra, I. Stals, P. Sandra, M. Claeysens, J. Van Beeumen, B. Devreese, *J. Chromatogr. A* 1058 (2004) 263.
- [20] Y. Satomi, Y. Shimonishi, T. Hase, T. Takao, *Rapid Commun. Mass Spectrom.* 18 (2004) 2983.
- [21] A. Harazono, N. Kawasaki, T. Kawanishi, T. Hayakawa, *Glycobiology* 15 (2005) 447.
- [22] M. Wuhler, C.A. Koeleman, C.H. Hokke, A.M. Deelder, *Anal. Chem.* 77 (2005) 886.
- [23] B.L. Schulz, N.H. Packer, N.G. Karlsson, *Anal. Chem.* 74 (2002) 6088.
- [24] N.L. Wilson, B.L. Schulz, N.G. Karlsson, N.H. Packer, *J. Proteome Res.* 1 (2002) 521.
- [25] L.A. Gennaro, D.J. Harvey, P. Vouros, *Rapid Commun. Mass Spectrom.* 17 (2003) 1528.
- [26] N.G. Karlsson, B.L. Schulz, N.H. Packer, *J. Am. Soc. Mass Spectrom.* 15 (2004) 659.
- [27] N.G. Karlsson, N.L. Wilson, H.J. Wirth, P. Dawes, H. Joshi, N.H. Packer, *Rapid Commun. Mass Spectrom.* 18 (2004) 2282.
- [28] M. Wuhler, C.A. Koeleman, A.M. Deelder, C.H. Hokke, *Anal. Chem.* 76 (2004) 833.
- [29] Y. Takegawa, K. Deguchi, S. Ito, S. Yoshioka, H. Nakagawa, S. Nishimura, *Anal. Chem.* 77 (2005) 2097.
- [30] S. Itoh, N. Kawasaki, M. Ohta, T. Hayakawa, *J. Chromatogr. A* 978 (2002) 141.
- [31] S. Itoh, N. Kawasaki, A. Harazono, N. Hashii, Y. Matsuishi, T. Kawanishi, T. Hayakawa, *J. Chromatogr. A* 1094 (2005) 105.
- [32] N. Kawasaki, M. Ohta, S. Hyuga, O. Hashimoto, T. Hayakawa, *Anal. Biochem.* 269 (1999) 297.
- [33] S. Itoh, N. Kawasaki, M. Ohta, M. Hyuga, S. Hyuga, T. Hayakawa, *J. Chromatogr. A* 968 (2002) 89.
- [34] N. Kawasaki, S. Itoh, M. Ohta, T. Hayakawa, *Anal. Biochem.* 316 (2003) 15.
- [35] C. Bordier, *J. Biol. Chem.* 256 (1981) 1604.
- [36] M.P. Lisanti, M. Sargiacomo, L. Graeve, A.R. Saltiel, E. Rodriguez-Boulan, *Proc. Natl. Acad. Sci. U.S.A.* 85 (1988) 9557.
- [37] B. Domon, C.E. Costello, *Glycoconjugate J.* 5 (1988) 397.
- [38] C. Sato, T. Matsuda, K. Kitajima, *J. Biol. Chem.* 277 (2002) 45299.



## Site-specific N-glycosylation analysis of human plasma ceruloplasmin using liquid chromatography with electrospray ionization tandem mass spectrometry

Akira Harazono\*, Nana Kawasaki, Satsuki Itoh, Noritaka Hashii,  
Akiko Ishii-Watabe, Toru Kawanishi, Takao Hayakawa

National Institute of Health Sciences, Division of Biological Chemistry and Biologicals, 1-18-1 Kami-yoga, Setagaya-Ku, Tokyo 158-8501, Japan

Received 8 June 2005

Available online 10 November 2005

### Abstract

Ceruloplasmin has ferroxidase activity and plays an essential role in iron metabolism. In this study, a site-specific glycosylation analysis of human ceruloplasmin (CP) was carried out using reversed-phase high-performance liquid chromatography with electrospray ionization tandem mass spectrometry (LC-ESI-MS/MS). A tryptic digest of carboxymethylated CP was subjected to LC-ESI-MS/MS. Product ion spectra acquired data-dependently were used for both distinction of the glycopeptides from the peptides using the carbohydrate B-ions, such as  $m/z$  204 (HexNAc) and  $m/z$  366 (HexHexNAc), and identification of the peptide moiety of the glycopeptide based on the presence of the b- and y-series ions derived from the peptide. Oligosaccharide composition was deduced from the molecular weight calculated from the observed mass of the glycopeptide and theoretical mass of the peptide. Of the seven potential N-glycosylation sites, four (Asn119, Asn339, Asn378, and Asn743) were occupied by a sialylated biantennary or triantennary oligosaccharide with fucose residues (0, 1, or 2). A small amount of sialylated tetraantennary oligosaccharide was detected. Exoglycosidase digestion suggested that fucose residues were linked to reducing end GlcNAc in biantennary oligosaccharides and to reducing end and/or  $\alpha$ 1–3 to outer arms GlcNAc in triantennary oligosaccharides and that roughly one of the antennas in triantennary oligosaccharides was  $\alpha$ 2–3 sialylated and occasionally  $\alpha$ 1–3 fucosylated at GlcNAc.

© 2005 Elsevier Inc. All rights reserved.

**Keywords:** Ceruloplasmin; Glycopeptide; Liquid chromatography-electrospray tandem mass spectrometry; Product ion spectrum; Exoglycosidase digestion

Ceruloplasmin (CP)<sup>1</sup> is a blue copper serum glycoprotein synthesized in the liver. CP has ferroxidase activity and plays an essential role in iron metabolism [1–4]. The primary structure of human CP has been determined by amino acid sequencing, and it is composed of a single poly-

peptide chain of 1046 amino acid residues [5]. The amino acid sequence was confirmed from complete cDNA sequence [6]. The major oligosaccharides in human CP were reported to be sialylated bi- and triantennary structures with or without a fucose residue [7,8]. Although four N-glycosylation sites (Asn119, Asn339, Asn378, and Asn743) were identified among seven potential sites [9], the heterogeneity of oligosaccharides was still unknown at each glycosylation site. CP is an acute phase reactant, and the serum concentration increases during inflammation, infection, and trauma [10]. It is known that the patterns of glycosylation are changed by inflammatory cytokines [11]. Several studies have reported that CP is a good diagnostic marker of solid malignant tumors [12,13] and that the CP glycoform might

\* Corresponding author. Fax: +81 3 3700 9084.

E-mail address: [harazono@nihs.go.jp](mailto:harazono@nihs.go.jp) (A. Harazono).

<sup>1</sup> Abbreviations used: CP, ceruloplasmin; LC-ESI-MS, liquid chromatography with electrospray ionization mass spectrometry; Hex, hexose; HexNAc, N-acetylhexosamine; LC-ESI-MS/MS, liquid chromatography with electrospray ionization tandem mass spectrometry; EDTA, ethylenediaminetetraacetic acid; TFA, trifluoroacetic acid; Q-TOF, quadrupole time-of-flight; TIC, total ion chromatogram; NeuAc, N-acetylneuraminic acid; GlcNAc, N-acetylglucosamine; Fuc, fucose.



be a valuable supplement [12]. Thus, it is important to conduct a site-specific glycosylation analysis of normal human CP.

One of the most effective techniques for determining the site-specific carbohydrate heterogeneity of glycoproteins is the mass spectrometric peptide mapping of proteolytic fragments of glycoproteins by liquid chromatography with electrospray ionization mass spectrometry (LC-ESI-MS) [14–19]. The specific detection of glycopeptides in a complex peptide mixture is generally achieved by monitoring specific carbohydrate fragment ions such as  $m/z$  204 (HexNAc) and  $m/z$  366 (HexHexNAc) produced by cone voltage fragmentation or by precursor ion scanning [15–19]. Because product ion spectra of glycopeptides show high abundant carbohydrate fragment ions and low abundant b- and y-series fragment ions derived from the peptide backbone [20,21], product ion spectra acquired data-dependently in liquid chromatography with electrospray ionization tandem mass spectrometry (LC-ESI-MS/MS) can be used for both the selection from the peptides and the identification of the glycopeptides [22]. MS in combination with specific exoglycosidase digestions allows us to obtain the site-specific information on anomericity and linkage of glycans [23]. In the current study, we conducted a site-specific glycosylation analysis of human CP and successfully determined glycosylation status and glycosylation profile at each N-glycosylation site.

## Materials and methods

### Materials

Acetonitrile, formic acid, and guanidine hydrochloride were purchased from Wako Pure Chemicals Industries (Osaka, Japan). Purified human CP was purchased from Calbiochem (San Diego, CA, USA). Modified trypsin was purchased from Promega (Madison, WI, USA).  $\alpha$ 2–3 Neuraminidase (EC 3.2.1.18) of *Macrobodella decora*, a recombinant form, and  $\alpha$ 1–3,4 fucosidase (EC 3.2.1.51) from *Xanthomonas* sp. were purchased from Calbiochem.  $\alpha$ 2–3,6,8,9 Neuraminidase (EC 3.2.1.18) of *Arthrobacter ureafaciens*, a recombinant form, and  $\beta$ 1–4 galactosidase (EC 3.2.1.23) were purchased from Sigma Chemical (St. Louis, MO, USA). The water used was obtained from a Milli-Q water system (Millipore, Bedford, MA, USA). All other reagents were of the highest quality available.

### Reduction and S-carboxymethylation of CP

CP (100  $\mu$ g) was dissolved in 270  $\mu$ l of 0.5 M Tris–HCl buffer (pH 8.5) that contained 8 M guanidine hydrochloride and 5 mM ethylenediaminetetraacetic acid (EDTA). After the addition of 2  $\mu$ l of 2-mercaptoethanol, the mixture was incubated for 2 h at 40 °C. Then 5.67 mg of monoiodoacetic acid was added, and the resulting mixture was incubated for 2 h at 40 °C in the dark. The reaction mixture was applied to a PD-10 column (Amersham Biosciences, Upp-

sala, Sweden) to remove the reagents, and the eluate was lyophilized.

### Trypsin digestion of CP

Reduced and carboxymethylated CP was redissolved in 100  $\mu$ l of 0.1 M Tris–HCl buffer (pH 8.0). An aliquot of 1  $\mu$ l of trypsin prepared as 1  $\mu$ g/ $\mu$ l was added to 50  $\mu$ l of CP solution (1:50, w/w), and the mixture was incubated for 16 h at 37 °C. The enzyme digestion was stopped by storing at –20 °C before analysis.

### HPLC of tryptic digest of CP

Tryptic digests (0.2 and 0.4  $\mu$ g) of human CP were analyzed by LC-ESI-MS/MS to identify the peptides and glycopeptides, respectively. HPLC was performed on a Paradigm MS 4 (Michrom BioResources, Auburn, CA, USA) equipped with a Magic C18 column (0.2  $\mu$ , 50 mm, Michrom BioResources). The eluents consisted of water containing 2% (v/v) acetonitrile and 0.1% (v/v) formic acid (pump A) and 90% acetonitrile and 0.1% formic acid (pump B). Trypsin-digested samples were loaded onto a microtrap (peptide captrap, Michrom BioResources). After a wash with 15  $\mu$ l H<sub>2</sub>O/CH<sub>3</sub>CN (98:2) with 0.1% trifluoroacetic acid (TFA), the trapping column was switched into line with the column. Samples were eluted with 5% of B for 10 min, followed by a linear gradient from 5 to 65% of B in 60 min at a flow rate of 2  $\mu$ l/min.

### ESI-Q-TOF-MS/MS

Mass spectrometric analyses were performed using a quadrupole time-of-flight (Q-TOF) mass spectrometer (QSTAR Pulsar, MDS Sciex, Toronto, Canada) equipped with a nano-electrospray ion source. The mass spectrometer was operated in the positive ion mode. The nanospray voltage was set at 2500 V. Mass spectra were acquired at  $m/z$  400–2000 or  $m/z$  1000–2000 for MS analysis and at  $m/z$  100–2000 for MS/MS analysis. After every regular MS acquisition, two MS/MS acquisitions against top two of the multiply charged molecular ions were performed (data-dependent acquisition). The precursor ions with the same  $m/z$  as acquired previously were excluded for 120 s. The collision energy was varied between 30 and 80 eV depending on the size and charge of the molecular ion. Accumulation times for the spectra were 1.0 and 2.0 s for MS and MS/MS, respectively. All peaks were resolved monoisotopically.

Tandem MS/MS data from LC-ESI-MS/MS runs were submitted to the search engine Mascot to identify the tryptic peptides of CP. One missed cleavage was allowed, and tolerances of 2.0 and 0.8 u mass were used for precursor and product ions, respectively. From the data for LC-ESI-MS/MS at  $m/z$  1000–2000, glycopeptide precursor ions were selected manually based on the presence of oligosaccharide oxonium ions such as  $m/z$  204 (HexNAc) and  $m/z$  366 (HexHexNAc). The glycopeptide ions were assigned based on

the presence of b- and y-series fragment ions of peptides of putative glycopeptides or molecular weight difference of sugar unit. The molecular weight of the carbohydrate in the glycopeptide was calculated from the molecular weights of the glycopeptide and the suggested peptide. The oligosaccharide composition and type were deduced from the molecular weight of the carbohydrate.

#### Oligosaccharide sequencing by exoglycosidase digestions

Trypsin in the digest of human CP was inactivated by boiling for 5 min at 100°C. Aliquots of the digest (4 µg) were digested in a volume of 20 µl for 12 h at 37°C in 50 mM sodium phosphate buffer (pH 5.0) using the following exoglycosidases alone or in combination: α2–3 neuraminidase, 20 mU/ml; α2–3,6,8,9 neuraminidase, 100 mU/ml; α1–3,4 fucosidase, 20 mU/ml; and β1–4 galactosidase, 30 mU/ml. Aliquots (0.08 µg) before and after exoglycosidase digestions were subjected to LC-ESI-MS at *m/z* 700 to 2000 in which MS/MS acquisition was not performed.

## Results

#### Peptide mapping of tryptic digest of human CP (LC-ESI-MS/MS in *m/z* range of 400–2000)

The amino acid sequence of human CP (National Center for Biotechnology Information protein database: P00450) is shown in Fig. 1. The tryptic peptides, including potential N-glycosylation sites, are shown in bold type. Trypsin can digest human CP into seven glycopeptides containing only one potential N-glycosylation site. To determine the glycosylation state at each glycosylation site, we performed mass spectrometric peptide mapping of the tryptic digest of CP. An aliquot of 0.2 µg of the tryptic digest was analyzed by

LC-ESI-MS/MS in the *m/z* range of 400–2000 (data not shown). When molecular ions with more than a single charge were detected, the product ion spectrum was acquired automatically. Peptide identification of each product ion spectrum was done using the Mascot search engine. More than 70% of the amino acid sequence was identified; identified amino acids of CP are underlined in Fig. 1. Three peptides containing the potential N-glycosylation site (Asn208, Asn569, and Asn907 [residues 197–218, 558–579, and 895–917, respectively]) were detected, whereas peptides containing the other N-glycosylation sites were not detected. Thus, Asn119, Asn339, Asn378, and Asn743 might be glycosylated.

#### Glycosylation analysis of human CP (LC-ESI-MS/MS in the *m/z* range of 1000–2000)

N-glycosylated peptides have relatively high molecular weights due to their oligosaccharide moiety. Because ions at lower *m/z* values can be detected in the *m/z* range of 400–2000, glycopeptide ions with higher *m/z* values might be missed to obtain product ion spectra. To detect glycopeptide ions preferentially, another LC-ESI-MS/MS analysis was carried out in the *m/z* range of 1000–2000 using an aliquot of 0.4 µg of the tryptic digest. Fig. 2A shows a total ion chromatogram (TIC) of a TOF-MS scan for the full scan *m/z* 1000–2000. Fig. 2B shows a TIC of the product ion scan. Because product ion spectra of glycopeptide precursor ions have abundant carbohydrate B-ions, *m/z* 204 (HexNAc), *m/z* 186 (HexNAc-H<sub>2</sub>O), *m/z* 366 (HexHexNAc), and *m/z* 292 (NeuAc), the extracted ion chromatogram at *m/z* 204.05–204.15 (HexNAc, 204.08) of the product ion scan is illustrated in Fig. 2C. The extracted ion chromatogram at *m/z* 204.05–204.15 of product ion spectra provides a useful indication of the selection of glycopeptide precursor ions. The glycopeptide ions were assigned based on an examination of product ion spectra using the information on amino acid sequences of the peptides containing a putative N-glycosylation site.

#### Identification of Asn119 glycopeptide

The product ion spectrum of 1366.6 (+3) at 26 min, labeled by A in Fig. 2C, is shown in Fig. 3A. There were abundant oligosaccharide oxonium ions such as *m/z* 204 (HexNAc), *m/z* 366 (HexHexNAc), *m/z* 186 (HexNAc-H<sub>2</sub>O), *m/z* 168 (HexNAc-2H<sub>2</sub>O), *m/z* 274 (NeuAc-H<sub>2</sub>O), and *m/z* 292 (NeuAc). Thus, this precursor ion was assigned as a glycopeptide. Several fragment ions consistent with b- and y-series fragment ions [24] derived from the peptide EHEGAIYPDN<sup>119</sup>TTDFQR (residues 110–125) were detected together with several deamidated (–17) or dehydrogenated (–18) b- and y-series ions and y-series ions with the GlcNAc residue. Thus, the peptide moiety EHEGAIYPDN<sup>119</sup>TTDFQR was suggested. The carbohydrate's molecular weight, 2223.0, was calculated by subtracting the theoretical molecular weight of the peptide (1891.8) from

KEKHYIIGII ETTWYASDH GEKKLISVDT EHSNIYLONG PDRIGRLYKK ALYLYQYTDET  
 FRTTIEKPVV LGFLGPIIKA ETGDKVYVHL KNLASRPYTF HSHGITYYKE HEGATYPPDNT<sup>119</sup>  
 TDFQADDKV YPGEQYTYML LATEEQSPGE GDGNCVTRIIY HSHIDAPKDI ASGLIGPLII  
 CKKDSLDKEK EKIHDFEYV MFSVVDENFS WYLEDNIRTY CSEPEKVDKD NEDFOESNRM  
 YSVNGYTFGS LPLGLMCAED RVKNYLFMG NGEVNVAIAFF HGQALTNKNY RIDTINLFPA  
 TLFDAYMVAQ NPGEMMLSCQ NLNHLKAGLO AFFOVQECNK<sup>119</sup> SSSKDNIRGK HVRHYIIAAE  
 EIIWNYAPSG IDIFTKENLT APGSDSAVFF EQGTRIGGS YKLVYREYT DASFTNRKER  
 GPVEEHLGIL GPVIAEVEGD TIRVTFHNKG AYPFLSIEPIG VRFNKNNEGT YSPNPNQPS  
 RSVPPSASHV APTEFTFYEV TVPKVEGPTN ADPVCLAKMY YSAVDPTKDI FTGLIGPMKI  
 CKKGLSHANG ROKDVKDFY LFPTVDFENE SLLLEDNIRM FTTAPDQVDK EDEDFOESNK  
 MHSMNGFMYG NQPGLTCKG DSVVYVLFSA GNEADVHGIV FSGNTYLWRG ERRDTANLFP  
 QTSLLTHMWP DTEGTFMVRG LTTDHYTGGM KOKYTVNOCR RQSEDSTFYL GERTYIIAAV  
 EVFWDYSPQR EWEKELHHLQ EQNVSNAFLD KGEFYIGSKY KKVYRQYTD STFRVPVERK  
 AEEEHLGILG PQLHADVDK VKIIFKNMAT RPYSIHAGV QTESSTVTPT LPGETLTYVM  
 KIPERSGAGT EDSACIPWAY YSTVDQVKDL YSGLIGPLIV CRPPYLKVFN PRRKLEFALL  
 FLVFDENESW YLDDNIKTYD DHPEKVNKDD EEFIESNKM AINGRMFGNL QCLTMHVQDE  
 VNWYLMGMGN EIDLHTVHFH GHSFOYKHRG VYSSDVFDFI PGTYQTLEMF PRTPGIWLLH  
 CHVTDIHAG METTYTVLQN EDTKSG

Fig. 1. Primary amino acid sequence of human CP (P00450). The tryptic peptides, including potential N-glycosylation sites, are shown in bold type. Tryptic peptides identified in the LC-ESI-MS/MS analysis are underlined. Cysteine residues are carboxymethylated. Identified N-glycosylation sites are indicated by arrow.

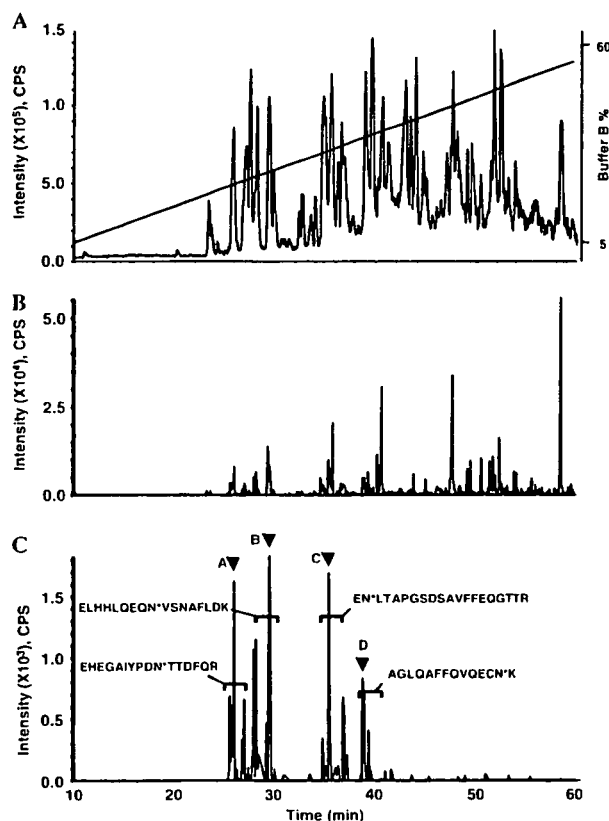


Fig. 2. LC-ESI-MS/MS in the  $m/z$  range of 1000–2000 of the tryptic digest of human CP. (A) TIC of the TOF-MS scan for the full-scan  $m/z$  1000–2000 and the HPLC gradient. (B) TIC of the product ion scan acquired data-dependently. (C) Extracted ion chromatogram at  $m/z$  204.05–204.15 of the product ion spectra. Brackets denote glycopeptide fraction and peptide sequences of the glycopeptides. Product ion spectra indicated by A–D are shown in Fig. 3.

the calculated molecular weight of the glycopeptide (4096.7) and adding the molecular weight of  $H_2O$  (18.0). The presence of product ions at  $m/z$  274 (NeuAc- $H_2O$ ) and  $m/z$  292 (NeuAc) suggested sialylation of the oligosaccharide. Thus, the carbohydrate's composition,  $[HexNAc]_4[Hex]_5[NeuAc]_2$ , was deduced.

#### Identification of Asn743 glycopeptide

The product ion spectrum of 1628.4 (+3) at 29 min, labeled by B in Fig. 2C, is shown in Fig. 3B. This precursor ion was assigned as a glycopeptide due to the presence of abundant oligosaccharide oxonium ions such as  $m/z$  204 (HexNAc),  $m/z$  366 (HexHexNAc), and  $m/z$  292 (NeuAc) in the product ion spectrum. Several fragment ions were consistent with theoretical b- and y-series fragment ions derived from the peptide ELHHLQEQN<sup>743</sup>VSN AFLDK (residues 735–751). Doubly charged ions of peptide ( $m/z$  1011.7), peptide + HexNAc ( $m/z$  1113.1), peptide + 2HexNAc ( $m/z$  1214.6), peptide + 2HexNAc + Hex ( $m/z$  1295.5), peptide + 2HexNAc + 2Hex ( $m/z$  1376.7), and peptide + 2HexNAc + 3Hex ( $m/z$  1457.5) showed the sequential fragmentation of the pentasaccharide carbohydrate core. The

carbohydrate's molecular weight, 2879.1, was calculated from the theoretical molecular weight of the peptide (2021.0) and the calculated molecular weight of the glycopeptide (4882.1). The carbohydrate's composition,  $[HexNAc]_5[Hex]_6[NeuAc]_3$ , was deduced from the molecular weight.

#### Identification of Asn378 glycopeptide

The product ion spectrum of 1444.6 (+3) at 35 min, labeled by C in Fig. 2C, is shown in Fig. 3C. Abundant oligosaccharide oxonium ions were detected, as were several fragment ions consistent with b- and y-series fragment ions derived from the peptide EN<sup>378</sup>LTAPGSDSAVFFEQGTTR (residues 377–391). The carbohydrate's molecular weight, 2222.9, was calculated from the theoretical molecular weight of the peptide (2126.0) and the calculated molecular weight of the glycopeptide (4330.9). Thus, the peptide moiety ENLTAPGSDSAVFFEQGTTR and the carbohydrate's composition,  $[HexNAc]_4[Hex]_5[NeuAc]_2$ , were suggested.

#### Identification of Asn339 glycopeptide

The product ion spectrum of 1282.6 (+3) at 39 min, labeled by D in Fig. 2C, is shown in Fig. 3C. The spectrum contains abundant oligosaccharide oxonium ions, and several fragment ions consistent with b- and y-series fragment ions derived from the peptide AGLQAFFQVQECN<sup>339</sup>K (residues 327–340) were detected. The product ion spectrum contains the ions of the peptide ( $m/z$  1640.8) and peptide + HexNAc ( $m/z$  1843.9) and several y-series fragment ions of the peptide with a GlcNAc residue. The carbohydrate's molecular weight, 2223.0, was calculated from the theoretical molecular weight of the peptide (1639.7) and the calculated molecular weight of the glycopeptide (3844.7). Thus, the peptide moiety AGLQAFFQVQECNK and the carbohydrate's composition,  $[HexNAc]_4[Hex]_5[NeuAc]_2$ , were suggested.

#### Heterogeneity of oligosaccharides at each glycosylation site

Glycopeptides with the potential N-glycosylation sites Asn119, Asn339, Asn378, and Asn743 were detected, whereas no glycopeptides containing the other sites (Asn208, Asn569, and Asn907) could be detected in this LC-ESI-MS/MS analysis. These findings suggest that Asn119, Asn339, Asn378, and Asn743 of human CP are glycosylated and that Asn208, Asn569, and Asn907 are not. Once a glycopeptide was identified, the other glycopeptides with the same peptide could be easily assigned because they were eluted at a similar retention time in the order of the number of NeuAc and had similar product ion spectra and molecular weight difference of sugar units. The oligosaccharide heterogeneity at each four N-glycosylation sites was determined by mass spectrum. For a representative example, the mass spectrum of the glycopeptides containing

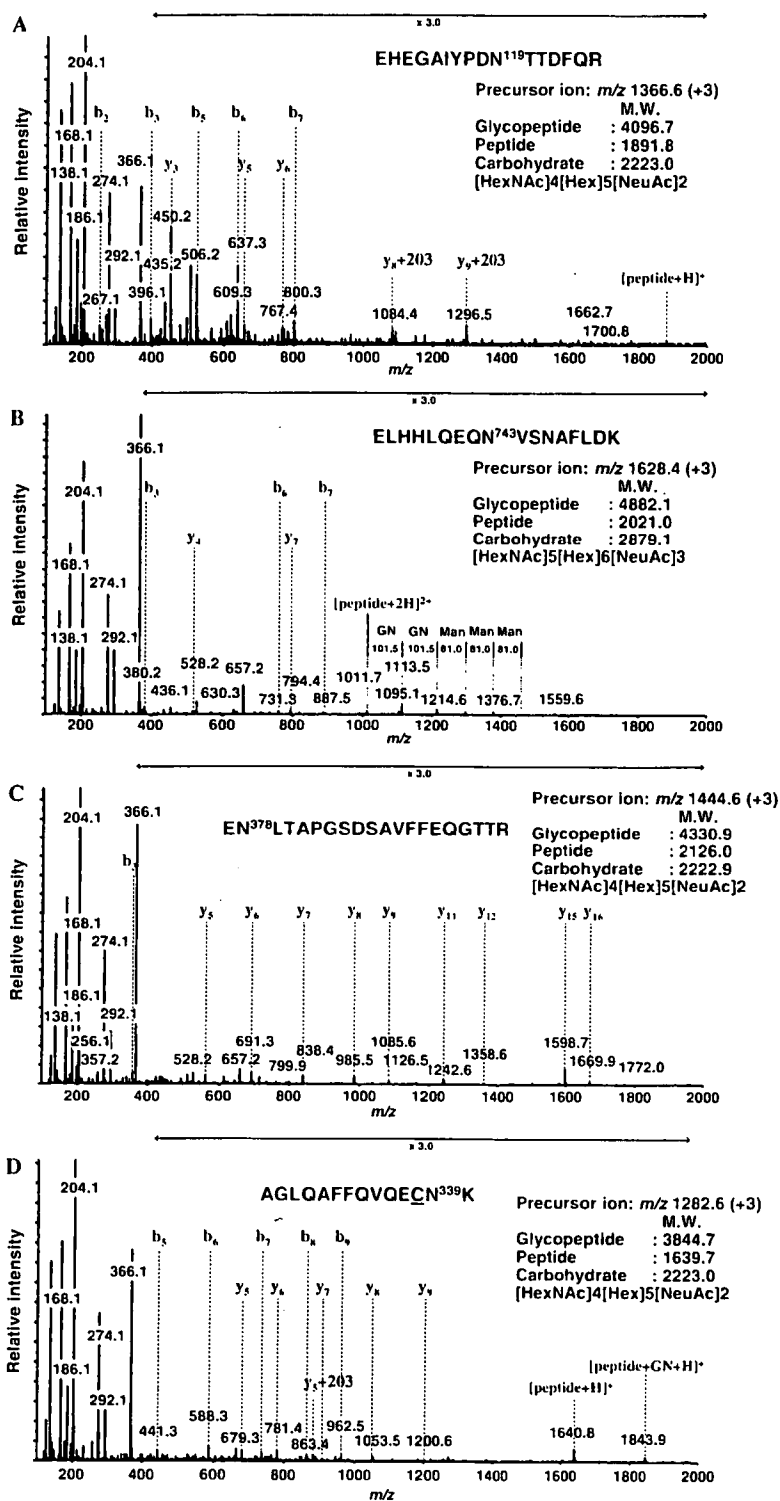


Fig. 3. Product ion spectra of  $m/z$  1366.6 (+3) at 26 min (A),  $m/z$  1628.4 (+3) at 29 min (B),  $m/z$  1444.6 (+3) at 35 min (C), and  $m/z$  1282.6 (+3) at 39 min (D) labeled by A, B, C, and D, respectively, in Fig. 2C. These spectra show abundant carbohydrate-derived ions at  $m/z$  168 (HexNAc-2H<sub>2</sub>O),  $m/z$  186 (HexNAc-H<sub>2</sub>O),  $m/z$  204 (HexNAc),  $m/z$  366 (HexHexNAc),  $m/z$  274 (NeuAc-H<sub>2</sub>O), and  $m/z$  292 (NeuAc). The b- and y-series fragment ions [24] derived from the peptide moiety were observed. The molecular weights of the oligosaccharide were calculated from the molecular weights of the glycopeptide and peptide, and the deduced oligosaccharide composition is presented. Cystein residue was carboxymethylated.

Asn743 at 27.5 to 31.5 min is shown Fig. 4. The results of glycosylation analysis are summarized in Table I. Deduced compositions of the oligosaccharides are estimated based on the calculated molecular weights of the oligosaccharides. Relative peak intensity was calculated by comparing triply charged glycopeptide ions. All glycosylation sites were occupied by at least three kinds of oligosaccharides, namely disialobiantennary structures ( $[\text{HexNAc}]_4[\text{Hex}]_5[\text{NeuAc}]_2$ ), disialobiantennary structures with fucose ( $[\text{HexNAc}]_4[\text{Hex}]_5[\text{NeuAc}]_2[\text{Fuc}]_1$ ), and trisialotriantennary structures ( $[\text{HexNAc}]_5[\text{Hex}]_6[\text{NeuAc}]_3$ ). Trisialotriantennary structures with one fucose or two fucoses ( $[\text{HexNAc}]_5[\text{Hex}]_6[\text{NeuAc}]_3[\text{Fuc}]_{1-2}$ ) were also detected at Asn119 and Asn743; furthermore, tetrasialotetraantennary structures with no fucose or one fucose ( $[\text{HexNAc}]_6[\text{Hex}]_7[\text{NeuAc}]_4[\text{Fuc}]_{0-1}$ ) were detected at Asn743.

#### Linkage analysis of oligosaccharides by exoglycosidase digestion

To elucidate the oligosaccharide structure in terms of sequence and linkage, aliquots of the tryptic digest were further digested with exoglycosidases. As a representative example, Fig. 5 shows integrated mass spectra during the periods at which Asn119 glycopeptides were eluted in LC-ESI-MS analyses before and after digestion with exoglycosidase arrays. Treatment with  $\alpha$ 2–3 neuraminidase removed one NeuAc residue from most of the triantennary structures ( $[\text{HexNAc}]_5[\text{Hex}]_6[\text{NeuAc}]_3[\text{Fuc}]_{0-2}$ ) and a small amount of biantennary structures ( $[\text{HexNAc}]_4[\text{Hex}]_5[\text{NeuAc}]_2[\text{Fuc}]_{0-1}$ ) (Fig. 5B). A minor amount of triantennary structures removed two NeuAc residues. Thus, it appears that most triantennary structures contain one  $\alpha$ 2–3-linked NeuAc. Treat-

ment with  $\alpha$ 2–3 neuraminidase +  $\beta$ 1–4 galactosidase removed all terminal galactose residues from the desialylated glycans without fucose residues but only partially digested terminal galactoses from the desialylated glycans with fucoses (Fig. 5C). The addition of  $\alpha$ 1–3,4 fucosidase to  $\alpha$ 2–3 neuraminidase +  $\beta$ 1–4 galactosidase treatment completely digested the remaining terminal galactose by releasing one fucose and one galactose (Fig. 5D). Thus, galactose residues are linked  $\beta$ 1–4 to GlcNAc, and undigestion of terminal galactose by  $\beta$ 1–4 galactosidase is due to attachment of fucose [25,26]. Because galactose was linked to GlcNAc in the  $\beta$ 1–4 position, the fucose removed with  $\alpha$ 1–3,4 fucosidase may be linked  $\alpha$ 1–3 to GlcNAc but not  $\alpha$ 1–4 to GlcNAc. These data strongly suggested that sialyl Lewis X structure was present in human CP. Sialyl Lewis X structure was present predominantly in triantennary oligosaccharides, but a small amount seemed to be present in biantennary oligosaccharides as well. The remaining fucose residue may be linked  $\alpha$ 1–6 to reducing end GlcNAc (core fucose).

Fig. 6 shows integrated mass spectra of Asn119, Asn743, Asn378, and Asn339 glycopeptides in LC-ESI-MS analysis following digestion with  $\alpha$ 2–3,6,8,9 neuraminidase +  $\beta$ 1–4 galactosidase. Treatment with  $\alpha$ 2–3,6,8,9 neuraminidase +  $\beta$ 1–4 galactosidase removed all NeuAc and then removed terminal galactoses in the outer arms without fucose. Thus, this treatment could differentiate glycoforms based on the location of fucose residues. Fucosylation occurred predominantly at reducing end GlcNAc in biantennary oligosaccharides and occurred at reducing end GlcNAc and/or outer arm GlcNAc in triantennary oligosaccharides. Mass spectra of Asn119 and Asn743 glycopeptides showed higher oligosaccharide heterogeneity, and a minor amount of tetraantennary glycans could be detected. The glycosylation profile

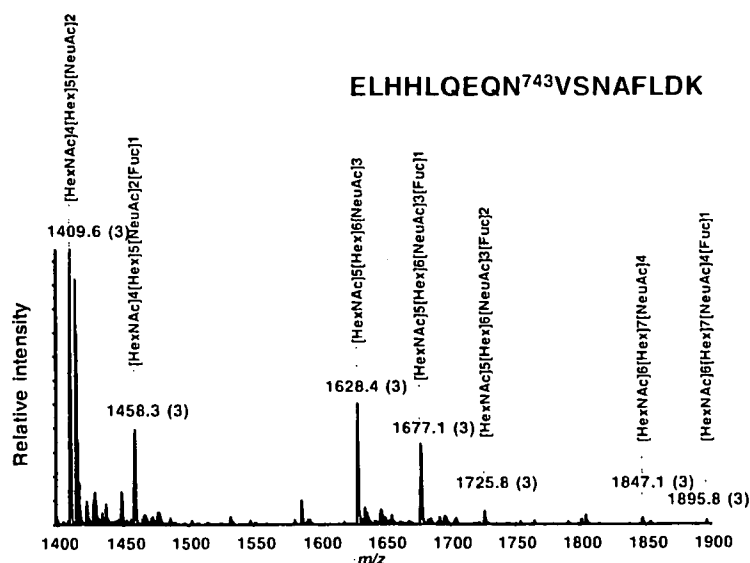


Fig. 4. Mass spectrum of the glycopeptides containing Asn743 eluting at 27.5–31.5 min from Fig. 2A. Deduced composition of the oligosaccharides is indicated based on the molecular weights of the oligosaccharides.

Table 1  
Results of site-specific glycosylation analysis of human CP

Retention time (min)	Glycopeptides		Calculated MW	Relative peak intensity <sup>a</sup> (%)	Peptide Sequence	Oligosaccharide		Theoretical MW	Composition <sup>b,c</sup>
	m/z	Charge				Calculated MW	Theoretical MW		
26	1415.3	+3	4242.8	52	EHEGAIYPDN <sup>119</sup> TTDFQR	2369.0	1891.8	2368.8	[HexNAc]4[Hex]5[NeuAc]2[Fuc]1
26	1366.6	+3	4096.7	100	EHEGAIYPDN <sup>119</sup> TTDFQR	2223.0	1891.8	2222.8	[HexNAc]4[Hex]5[NeuAc]2
27	1682.7	+3	5045.1	6	EHEGAIYPDN <sup>119</sup> TTDFQR	3171.3	1891.8	3171.1	[HexNAc]5[Hex]6[NeuAc]3[Fuc]2
27	1634.0	+3	4899.0	21	EHEGAIYPDN <sup>119</sup> TTDFQR	3025.2	1891.8	3025.1	[HexNAc]5[Hex]6[NeuAc]3[Fuc]1
27	1225.8	+4	4899.0						
27	1585.3	+3	4753.0	24	EHEGAIYPDN <sup>119</sup> TTDFQR	2879.2	1891.8	2879.0	[HexNAc]5[Hex]6[NeuAc]3
27	1189.3	+4	4753.0						
28	1458.3	+3	4372.0	35	ELHHLQEQN <sup>743</sup> YSNAFLDK	2369.0	2021.0	2368.8	[HexNAc]4[Hex]5[NeuAc]2[Fuc]1
28	1409.6	+3	4225.9	100	ELHHLQEQN <sup>743</sup> YSNAFLDK	2222.9	2021.0	2222.8	[HexNAc]4[Hex]5[NeuAc]2
28	1057.5	+4	4225.9						
29	1725.8	+3	5174.5	5	ELHHLQEQN <sup>743</sup> YSNAFLDK	3171.5	2021.0	3171.1	[HexNAc]5[Hex]6[NeuAc]3[Fuc]2
29	1294.6	+4	5174.2						
29	1677.1	+3	5028.2	29	ELHHLQEQN <sup>743</sup> YSNAFLDK	3025.3	2021.0	3025.1	[HexNAc]5[Hex]6[NeuAc]3[Fuc]1
29	1258.1	+4	5028.2						
29	1628.4	+3	4882.1	43	ELHHLQEQN <sup>743</sup> YSNAFLDK	2879.1	2021.0	2879.0	[HexNAc]5[Hex]6[NeuAc]3
29	1221.5	+4	4882.1						
31 <sup>d</sup>	1895.8	+3	5684.4	2	ELHHLQEQN <sup>743</sup> YSNAFLDK	3681.4	2021.0	3681.3	[HexNAc]6[Hex]7[NeuAc]4[Fuc]1
31 <sup>e</sup>	1422.1	+4	5684.3						
31 <sup>d</sup>	1847.1	+3	5538.4	3	ELHHLQEQN <sup>743</sup> YSNAFLDK	3535.4	2021.0	3535.2	[HexNAc]6[Hex]7[NeuAc]4
31	1385.6	+4	5538.3						
35 <sup>d</sup>	1493.3	+3	4477.0	6	EN <sup>378</sup> LTAPGSDSAVFEEQGTTTR	2369.0	2126.0	2368.8	[HexNAc]4[Hex]5[NeuAc]2[Fuc]1
35	1444.6	+3	4330.9	100	EN <sup>378</sup> LTAPGSDSAVFEEQGTTTR	2222.9	2126.0	2222.8	[HexNAc]4[Hex]5[NeuAc]2
37	1712.1	+3	5133.2	8	EN <sup>378</sup> LTAPGSDSAVFEEQGTTTR	3025.2	2126.0	3025.1	[HexNAc]5[Hex]6[NeuAc]3[Fuc]1
37	1284.3	+4	5133.2						
37	1663.4	+3	4987.1	23	EN <sup>378</sup> LTAPGSDSAVFEEQGTTTR	2879.2	2126.0	2879.0	[HexNAc]5[Hex]6[NeuAc]3
37	1247.8	+4	4987.2						
39	1331.3	+3	3990.8	14	AGLQAFFQVQECN <sup>319</sup> K	2369.1	1639.7	2368.8	[HexNAc]4[Hex]5[NeuAc]2[Fuc]1
39	1923.4	+2	3844.7						
39	1282.6	+3	3844.7	100	AGLQAFFQVQECN <sup>319</sup> K	2223.0	1639.7	2222.8	[HexNAc]4[Hex]5[NeuAc]2
41	1501.3	+3	4500.8	6	AGLQAFFQVQECN <sup>319</sup> K	2879.2	1639.7	2879.0	[HexNAc]5[Hex]6[NeuAc]3

*Note.* All masses are monoisotopic. Cysteine residue was carboxymethylated.

<sup>a</sup> Relative peak intensity was calculated by comparing same charge state glycopeptide ions. The intensity of the glycoform with maximum at each glycosylation site was taken as 100%.

<sup>b</sup> The oligosaccharide composition was deduced from the molecular weight of the oligosaccharide.

<sup>c</sup> The glycopeptide ions adducted by NH<sub>4</sub><sup>+</sup> or Na<sup>+</sup> were excluded.

<sup>d</sup> Product ion spectra of these molecular ions were not acquired. However, these were considered glycopeptides because of a molecular weight difference of 146 (Fuc) and the same retention time as other glycopeptides.

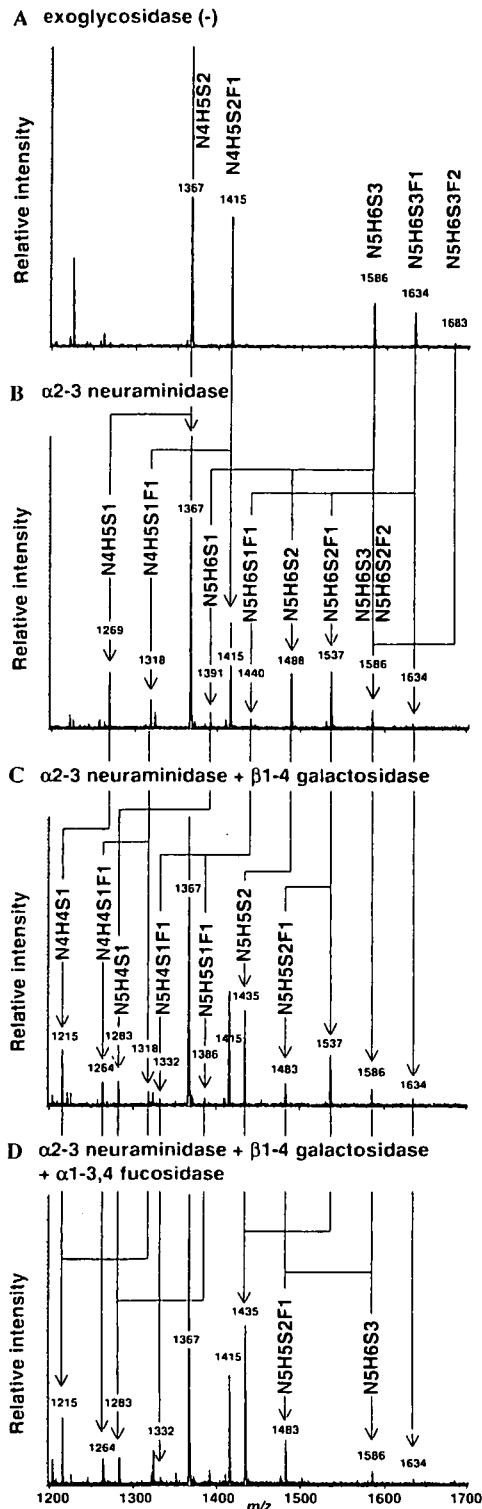


Fig. 5. LC-ESI mass spectra of the glycopeptides containing Asn119 digested with the following exoglycosidases: (A) exoglycosidase (-); (B)  $\alpha$ 2-3 neuraminidase; (C)  $\alpha$ 2-3 neuraminidase +  $\beta$ 1-4 galactosidase; (D)  $\alpha$ 2-3 neuraminidase +  $\beta$ 1-4 galactosidase +  $\alpha$ 1-3,4 fucosidase. Arrows between panels A and B, panels B and C, and panels C and D correspond to the digestion of NeuAc, Gal, and Gal+Fuc, respectively. H, hexose; N, N-acetylhexosamine; F, fucose; S, N-acetylneuraminic acid.

of Asn378 glycopeptides showed lower core fucosylation, and that of Asn339 glycopeptides showed lower branching. These glycosylation profiles provided the heterogeneity of fucose linkage and the number of arms at each glycosylation site in human CP.

## Discussion

A site-specific glycosylation analysis of human CP was conducted using LC-ESI-MS/MS, where product ion spectra were acquired in a data-dependent manner. The collision energy for the product ion scan was adjusted from 30 to 80 eV depending on the size and charge of the precursor ion. Under these conditions, peptide precursor ions were degraded and produced b- and y-series fragment ions derived from the amino acid sequence. Glycopeptide precursor ions produced abundant carbohydrate ions ( $m/z$  204, 186, 168, and 366) together with several low intensity b- and y-series fragment ions derived from the amino acid sequence [20,21]. Thus, product ion spectra of glycopeptides are readily distinguishable from those of peptides by such carbohydrate marker ions, and the peptide moiety in the glycopeptide could be deduced from the product ions that were consistent with the expected fragment ions derived from the peptide containing the N-glycosylation site. It is known that the glycopeptide ions are more labile than peptide ions and produce consecutive monosaccharide/polysaccharide losses at much lower collision energy, and this would provide information about branching and fucose location [18]. However, we used relatively high collision energy in this site-specific glycosylation analysis to identify the peptide ions in parallel with the detection and identification of the glycopeptide ions.

Protein coverage of more than 70% in human CP was obtained in the LC-ESI-MS/MS analysis with the  $m/z$  range of 400–2000 (for peptide mapping). The heterogeneity at four potential N-glycosylation sites was determined in the  $m/z$  range of 1000–2000 (glycosylation analysis). We could detect all of the potential glycosylation sites as either glycopeptides or nonglycosylated peptides. Peptides containing the potential N-glycosylation site Asn208, Asn569, or Asn907 were detected in nonglycosylated but not glycosylated forms. Peptides with the potential N-glycosylation site Asn119, Asn339, Asn378 or Asn743 were detected in glycosylated but not nonglycosylated forms. These findings indicate that Asn119, Asn339, Asn378, and Asn743 of human CP are glycosylated and that Asn208, Asn569, and Asn907 are not. Human CP was reported to have no O-linked glycosylation [8]. No information on O-glycosylation was obtained from this analysis. These results are consistent with a previous study determining the glycosylation sites of human CP [9].

Heterogeneity of oligosaccharides was determined at each of four glycosylation sites. Disialobiantennary structures with no fucose or one fucose ( $[\text{HexNAc}]_4 [\text{Hex}]_5 [\text{NeuAc}]_2 [\text{Fuc}]_{0-1}$ ) and trisialotriantennary structures

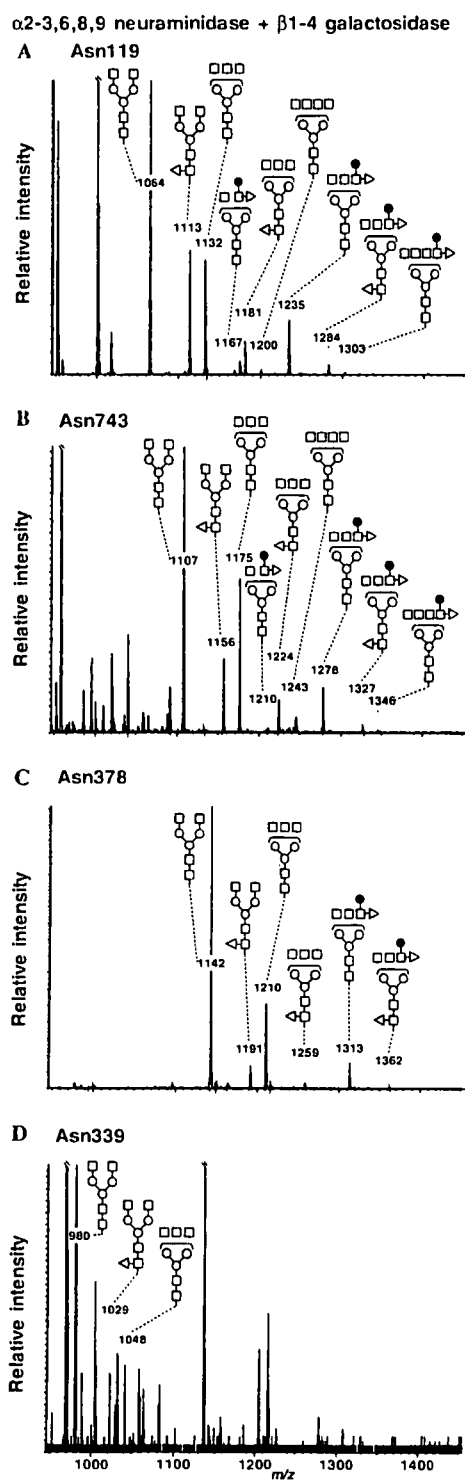


Fig. 6. LC-ESI mass spectra of the glycopeptides containing Asn119 (A), Asn743 (B), Asn378 (C), and Asn339 (D) after digestion with  $\alpha$ 2-3,6,8,9 neuraminidase +  $\beta$ 1-4 galactosidase. Glycosylation profiles showed different degrees of branching and fucosylation at core GlcNAc and outer arm GlcNAc between glycosylation sites. Open circles, mannose; closed circles, galactose; open squares, *N*-acetyl glucosamine; open triangles, fucose.

([HexNAc]<sub>5</sub>[Hex]<sub>6</sub>[NeuAc]<sub>3</sub>) were observed at all sites. These dominant oligosaccharides were consistent with structures published previously [7,8]. Furthermore, we detected trisialotriantennary structures with one fucose ([HexNAc]<sub>5</sub>[Hex]<sub>6</sub>[NeuAc]<sub>3</sub>[Fuc]<sub>1</sub>) at Asn119, Asn378, and Asn743, trisialotriantennary structures with two fucoses ([HexNAc]<sub>5</sub>[Hex]<sub>6</sub>[NeuAc]<sub>3</sub>[Fuc]<sub>2</sub>) at Asn119 and Asn743, and tetrasialotetraantennary structures with no fucose or one fucose ([HexNAc]<sub>6</sub>[Hex]<sub>7</sub>[NeuAc]<sub>4</sub>[Fuc]<sub>0-1</sub>) at Asn743.

To determine the linkage of fucose and NeuAc, exoglycosidase digestions were performed. Treatment with  $\alpha$ 2-3 neuraminidase suggested that roughly one antenna of triantennary glycans was linked by NeuAc in the  $\alpha$ 2-3 position. This is consistent with the previous findings that NeuAc is linked  $\alpha$ 2-3 to the Gal $\beta$ 1-4GlcNAc $\beta$ 1-4Man $\alpha$ 1-3Man $\beta$ 1-4GlcNAc $\beta$ 1-4GlcNAc group in the triantennary glycan in human CP [7,8]. Results from  $\alpha$ 2-3 neuraminidase +  $\beta$ 1-4 galactosidase treatments with or without  $\alpha$ 1-3,4 fucosidase suggested that fucose residues were linked to reducing end GlcNAc and/or outer arm GlcNAc in the  $\alpha$ 1-3 position in the antenna where NeuAc is linked to galactose in the  $\alpha$ 2-3 position. These findings indicated that human CP contains a certain amount of sialyl Lewis X structure in triantennary glycans. Treatment with  $\alpha$ 2-3,6,8,9 neuraminidase +  $\beta$ 1-4 galactosidase reveals the heterogeneity of the location of fucosylation as well as the number of arms. Although relative peak intensity does not express the relative amount of each glycan due to the different ionization efficiencies, the mass spectra showed the difference in fucosylation pattern and number of arms among sites.

No asialo oligosaccharides were detected in this analysis. It is known that desialylated CP is rapidly cleared from the circulation by the asialoglycoprotein receptor within the parenchymal cells of liver [27,28]. It is possible that desialylated CP might be cleared immediately by the liver.

Although the *N*-linked carbohydrate structures linked to human CP have been studied, only a few carbohydrate structures have been reported and site-specific characterization of these oligosaccharides has not been described. To determine the glycosylation state at each glycosylation site, the tryptic digest was examined by LC-ESI-MS/MS, where product ion spectra were acquired data-dependently. Glycopeptide ions were assigned based on the product ion spectra. Fucose and NeuAc linkages were determined by exoglycosidase digestions. Our data successfully provided comprehensive information on the site-specific *N*-linked oligosaccharides in human CP. This method is a powerful technique for elucidating the glycosylation of a biological sample.

#### Acknowledgments

This study was supported by a Grant-in-Aid for Research on Health Sciences focusing on Drug Innovation from the Japan Health Sciences Foundation.



## References

- [1] S. Osaki, D.A. Johnson, E. Frieden, The possible significance of the ferrous oxidase activity of ceruloplasmin in normal human serum, *J. Biol. Chem.* 241 (1966) 2746–2751.
- [2] K. Yoshida, K. Furihata, S. Takeda, A. Nakamura, K. Yamamoto, H. Morita, S. Hiyamuta, S. Ikeda, N. Shimizu, N. Yanagisawa, A mutation in the ceruloplasmin gene is associated with systemic hemosiderosis in humans, *Nat. Genet.* 9 (1995) 267–272.
- [3] Z.L. Harris, Y. Takahashi, H. Miyajima, M. Serizawa, R.T. MacGillivray, J.D. Gitlin, Aceruloplasminemia: molecular characterization of this disorder of iron metabolism, *Proc. Natl. Acad. Sci. USA* 92 (1995) 2539–2543.
- [4] Z.L. Harris, A.P. Durley, T.K. Man, J.D. Gitlin, Targeted gene disruption reveals an essential role for ceruloplasmin in cellular iron efflux, *Proc. Natl. Acad. Sci. USA* 96 (1996) 10812–10817.
- [5] N. Takahashi, T.L. Ortel, F.W. Putnam, Single-chain structure of human ceruloplasmin: the complete amino acid sequence of the whole molecule, *Proc. Natl. Acad. Sci. USA* 81 (1984) 390–394.
- [6] M.L. Koschinsky, W.D. Funk, B.A. van Oost, R.T. MacGillivray, Complete cDNA sequence of human preceruloplasmin, *Proc. Natl. Acad. Sci. USA* 83 (1986) 5086–5090.
- [7] K. Yamashita, C.J. Liang, S. Funakoshi, A. Kobata, Structural studies of asparagine-linked sugar chains of human ceruloplasmin. Structural characteristics of the triantennary complex type sugar chains of human plasma glycoproteins, *J. Biol. Chem.* 256 (1981) 1283–1289.
- [8] M. Endo, K. Suzuki, K. Schmid, B. Fournet, Y. Karamanos, J. Montreuil, L. Dorland, H. van Halbeek, J.F. Vliegthart, The structures and microheterogeneity of the carbohydrate chains of human plasma ceruloplasmin: a study employing 500-MHz <sup>1</sup>H-NMR spectroscopy, *J. Biol. Chem.* 257 (1982) 8755–8760.
- [9] N. Takahashi, Y. Takahashi, T.L. Ortel, J.N. Lozier, N. Ishioka, F.W. Putnam, Purification of glycopeptides of human plasma proteins by high-performance liquid chromatography, *J. Chromatogr.* 317 (1984) 11–26.
- [10] R.J. Cousins, Absorption, transport, and hepatic metabolism of copper and zinc: special reference to metallothionein and ceruloplasmin, *Physiol. Rev.* 65 (1985) 238–309.
- [11] A. Mackiewicz, M.K. Ganapathi, D. Schultz, I. Kushner, Monokines regulate glycosylation of acute-phase proteins, *J. Exp. Med.* 166 (1987) 253–258.
- [12] J.E. Hansen, J. Iversen, A. Lihme, T.C. Bog-Hansen, Acute phase reaction, heterogeneity, and microheterogeneity of serum proteins as nonspecific tumor markers in lung cancer, *Cancer* 60 (1987) 1630–1635.
- [13] A. Senra Varela, J.J. Lopez Saez, D. Quintela Senra, Serum ceruloplasmin as a diagnostic marker of cancer, *Cancer Lett.* 121 (1997) 139–145.
- [14] V. Ling, A.W. Guzzetta, E. Canova-Davis, J.T. Stults, W.S. Hancock, T.R. Covey, B.I. Shushan, Characterization of the tryptic map of recombinant DNA derived tissue plasminogen activator by high-performance liquid chromatography-electrospray ionization mass spectrometry, *Anal. Chem.* 63 (1991) 2909–2915.
- [15] S.A. Carr, M.J. Huddleston, M.F. Bean, Selective identification and differentiation of N- and O-linked oligosaccharides in glycoproteins by liquid chromatography–mass spectrometry, *Protein Sci.* 2 (1993) 183–196.
- [16] M.J. Huddleston, M.F. Bean, S.A. Carr, Collisional fragmentation of glycopeptides by electrospray ionization LC/MS and LC/MS/MS: methods for selective detection of glycopeptides in protein digests, *Anal. Chem.* 65 (1993) 877–884.
- [17] P.A. Schindler, C.A. Settineri, X. Collet, C.J. Fielding, A.L. Burlingame, Site-specific detection and structural characterization of the glycosylation of human plasma proteins lecithin:cholesterol acyltransferase and apolipoprotein D using HPLC/electrospray mass spectrometry and sequential glycosidase digestion, *Protein Sci.* 4 (1995) 791–803.
- [18] M.A. Ritchie, A.C. Gill, M.J. Deery, K. Lilley, Precursor ion scanning for detection and structural characterization of heterogeneous glycopeptide mixtures, *J. Am. Soc. Mass Spectrom.* 13 (2002) 1065–1077.
- [19] F. Wang, A. Nakouzi, R.H. Angeletti, A. Casadevall, Site-specific characterization of the N-linked oligosaccharides of a murine immunoglobulin M by high-performance liquid chromatography/electrospray mass spectrometry, *Anal. Biochem.* 314 (2003) 266–280.
- [20] J.F. Nemeth, G.P. Hochgesang Jr., L.J. Marnett, R.M. Caprioli, Characterization of the glycosylation sites in cyclooxygenase-2 using mass spectrometry, *Biochemistry* 40 (2001) 3109–3116.
- [21] O. Krokhin, W. Ens, K.G. Standing, J. Wilkins, H. Perreault, Site-specific N-glycosylation analysis: matrix-assisted laser desorption/ionization quadrupole–quadrupole time-of-flight tandem mass spectral signatures for recognition and identification of glycopeptides, *Rapid Commun. Mass Spectrom.* 18 (2004) 2020–2030.
- [22] A. Harazono, N. Kawasaki, T. Kawanishi, T. Hayakawa, Site-specific glycosylation analysis of human apolipoprotein B100 using LC/ESI MS/MS, *Glycobiology* 15 (2005) 447–462.
- [23] C.W. Sutton, J.A. O'Neill, J.S. Cottrell, Site-specific characterization of glycoprotein carbohydrates by exoglycosidase digestion and laser desorption mass spectrometry, *Anal. Biochem.* 218 (1994) 34–46.
- [24] P. Roepstorff, J. Fohlman, Proposal for a common nomenclature for sequence ions in mass spectra of peptides, *Biomed. Mass Spectrom.* 11 (1984) 601.
- [25] K. Maemura, M. Fukuda, Poly-N-acetylactosaminyl O-glycans attached to leukosialin: the presence of sialyl Le(x) structures in O-glycans, *J. Biol. Chem.* 267 (1992) 24379–24386.
- [26] S. Hemmerich, S.D. Rosen, 6'-Sulfated sialyl Lewis X is a major capping group of GlyCAM-1, *Biochemistry* 33 (1994) 4830–4835.
- [27] C.J. Van Den Hamer, A.G. Morell, I.H. Scheinberg, J. Hickman, G. Ashwell, Physical and chemical studies on ceruloplasmin: IX. The role of galactosyl residues in the clearance of ceruloplasmin from the circulation, *J. Biol. Chem.* 245 (1970) 4397–4402.
- [28] A.G. Morell, G. Gregoriadis, I.H. Scheinberg, J. Hickman, G. Ashwell, The role of sialic acid in determining the survival of glycoproteins in the circulation, *J. Biol. Chem.* 246 (1971) 1461–1467.

# Specific detection of Lewis x-carbohydrates in biological samples using liquid chromatography/multiple-stage tandem mass spectrometry

Noritaka Hashii<sup>1,2</sup>, Nana Kawasaki<sup>1,2\*</sup>, Satsuki Itoh<sup>1</sup>, Akira Harazono<sup>1</sup>, Yukari Matsuishi<sup>1,2</sup>, Takao Hayakawa<sup>3</sup> and Toru Kawanishi<sup>1</sup>

<sup>1</sup>Division of Biological Chemistry and Biologicals, National Institute of Health Sciences, 1-18-1 Kamiyoga, Setagaya-ku, Tokyo 158-8501, Japan

<sup>2</sup>Core Research for Evolutional Science and Technology (CREST) of Japan Science and Technology Agency (JST), Kawaguchi Center Building, 4-1-8 Hon-cho, Kawaguchi, Saitama 332-0012, Japan

<sup>3</sup>Pharmaceutical and Medical Devices Agency, 3-3-2 Kasumigaseki, Chiyoda-ku, Tokyo 100-0013, Japan

Received 14 July 2005; Revised 5 September 2005; Accepted 8 September 2005

The Lewis x structure [Le<sup>x</sup>, Gal $\beta$ 1-4(Fuc $\alpha$ 1-3)GlcNAc] motif is one of the tumor antigens and plays an important role in oncogenesis, development, cellular differentiation and adhesion. The detection of Le<sup>x</sup>-carbohydrates and their structural analysis are necessary to clarify the role of Le<sup>x</sup> in several biological events. Mass spectrometry has been preferably used for the structural analysis of carbohydrates. Especially, collision-induced dissociation (CID) tandem mass spectrometry (MS/MS), which causes a glycosidic bond cleavage, is used for carbohydrate sequencing. However, Le<sup>x</sup> cannot be identified by MS/MS due to the existence of the positional isomers, such as Lewis a [Gal $\beta$ 1-3( $\alpha$ 1-4Fuc)GlcNAc]. In the present study, we demonstrate the specific detection of Le<sup>x</sup>-carbohydrates in a biological sample by using multiple-stage MS/MS (MS<sup>n</sup>). Using pyridylaminated oligosaccharides bearing Le<sup>x</sup>, we found that the Le<sup>x</sup>-motif yields a cross-ring fragment by the cleavage of a bond between C-3 and C-4 of GlcNAc in Gal(Fuc)GlcNAc. The Le<sup>x</sup>-specific cross-ring fragment ion at *m/z* 259 was effectively detected by sequential scans, consisting of a full MS<sup>1</sup> scan, data-dependent CID MS<sup>2</sup> scan, MS<sup>3</sup> of [Gal(Fuc)GlcNAc+Na]<sup>+</sup> at *m/z* 534, and MS<sup>4</sup> of [GalGlcNAc+Na]<sup>+</sup> at *m/z* 388. The sequential scan was applied to *N*-linked oligosaccharide profiling using a LC/ESI-MS<sup>n</sup> system equipped with a graphitized carbon column. We successfully detected the Le<sup>x</sup>-motif and elucidated the structures of several Le<sup>x</sup> and Lewis y [(Fuc $\alpha$ 1-2)Gal $\beta$ 1-4(Fuc $\alpha$ 1-3)GlcNAc] oligosaccharides in the murine kidney used as a model tissue. Our method is expected to be a powerful tool for the specific detection of the Le<sup>x</sup>-motif, and structural elucidation of Le<sup>x</sup>-carbohydrates in biological samples. Copyright © 2005 John Wiley & Sons, Ltd.

The Lewis x structure [Le<sup>x</sup>, Gal $\beta$ 1-4(Fuc $\alpha$ 1-3)GlcNAc] is one of the tumor antigens, and plays an important role in oncogenesis<sup>1,2</sup> (abbreviations used here are: Gal, galactose; Fuc, fucose; GlcNAc, *N*-acetylglucosamine). Particularly, sialylated Le<sup>x</sup> is used as a marker of lung, pancreas and uterus tumors.<sup>3</sup> Le<sup>x</sup> and its derivatives are also known to be oligosaccharide ligands of some endothelial receptors, such as the selectins and the scavenger receptor, C-type lectin,<sup>4,5</sup> and affect embryonic development, cellular differentiation and adhesion.<sup>6,7</sup> However, the structural details of the oligosaccharides attached to the Le<sup>x</sup> structure (Le<sup>x</sup>-oligosaccharide) are still unclear. Le<sup>x</sup> structure-specific detection and elucidation

methods are necessary for the diagnosis of tumors and a study on the role of Le<sup>x</sup> on various biological events.

Mass spectrometry (MS) has become very popular for the structural analysis of oligosaccharides. Low-energy collision-induced dissociation (CID) tandem mass spectrometry (MS/MS), which generates B/Y-series ions by glycosidic bond cleavage, is preferably used for oligosaccharide sequencing.<sup>8–13</sup> However, the detection of Le<sup>x</sup> by MS/MS is still challenging due to the presence of its positional isomer, Lewis a [Le<sup>a</sup>, Gal $\beta$ 1-3(Fuc $\alpha$ 1-4)GlcNAc]. The structural difference between Le<sup>x</sup> and Le<sup>a</sup> is the linkage at positions 3 or 4 of the non-reducing terminal fucose and galactose to GlcNAc (Fig. 1). For the linkage analysis, multiple-stage MS/MS (MS<sup>n</sup>) pattern-matching, in which the oligosaccharide structure can be deduced from intensity ratios of fragment ions generated by MS<sup>n</sup>, has recently been reported,<sup>14–16</sup> however, this method needs an identical analytical condition and various oligosaccharide standards. As an alternative method, the cross-ring fragmentation caused by MS<sup>n</sup> is

\*Correspondence to: N. Kawasaki, Division of Biological Chemistry and Biologicals, National Institute of Health Sciences, 1-18-1 Kamiyoga, Setagaya-ku, Tokyo 158-8501, Japan.

E-mail: nana@nihs.go.jp

Contract/grant sponsor: Ministry of Health Labor and Welfare, and Core Research for the Evolutional Science and Technology Program, Japan Science and Technology Corp.

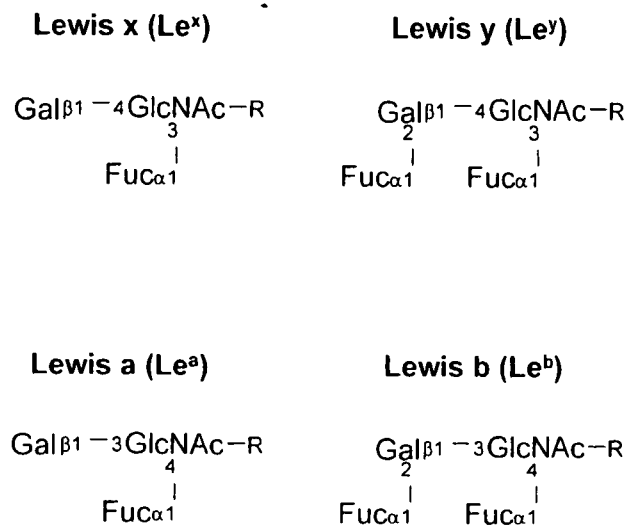


**Figure 1.** Structures of Lewis a, b, x and y.

sometimes used.<sup>10,17,18</sup> Meisen *et al.*<sup>19</sup> demonstrated that  $\alpha 2$ -6-linked *N*-acetylneuraminic acid (NeuNAc) can be distinguished from  $\alpha 2$ -3-linked NeuNAc based on structure-specific cross-ring fragment ions generated by low-energy CID MS<sup>2</sup> in the negative ion mode. Le<sup>x</sup> could be expected to be distinguished from its positional isomers by cross-ring fragmentation.

In this study, we demonstrate the specific detection of Le<sup>x</sup>-carbohydrates in a biological sample by using MS<sup>n</sup>. Using pyridylaminated oligosaccharides bearing Le<sup>x</sup>, we found that the Le<sup>x</sup>-motif yields a cross-ring fragment by the cleavage of a bond between C-3 and C-4 of GlcNAc in Gal(Fuc)GlcNAc. The Le<sup>x</sup>-specific cross-ring fragment ion at *m/z* 259 was effectively detected by sequential scans, consisting of a full MS<sup>1</sup> scan, data-dependent CID MS<sup>2</sup>-scan, MS<sup>3</sup> of [Gal(Fuc)GlcNAc+Na]<sup>+</sup> at *m/z* 534, and MS<sup>4</sup> of [GalGlcNAc+Na]<sup>+</sup> at *m/z* 388 using nano-electrospray ionization-ion trap mass spectrometry (nanoESI-ITMS) in positive ion mode. Then, sequential MS<sup>1-4</sup> scanning for the Le<sup>x</sup>-characteristic ions was applied for *N*-linked oligosaccharide profiling using an LC/ESI-ITMS instrument equipped with a graphitized carbon column (GCC), by which diverse oligosaccharides, including isomers, can be separated. We successfully detected the Le<sup>x</sup>-motif and subsequently elucidated the entire structure of Le<sup>x</sup>-oligosaccharides in the model tissue, murine kidney, in which Le<sup>x</sup>-oligosaccharides are abundantly present.<sup>20</sup>

## EXPERIMENTAL

### Materials

2-Aminopyridine (PA)-labeled pentasaccharides bearing Le<sup>x</sup> (oligosaccharide I, Fig. 2(A)) or Le<sup>a</sup> (oligosaccharide II, Fig. 2(B)), and the asialotriantennary oligosaccharide bearing Le<sup>x</sup> (oligosaccharide III, Fig. 2(C)), were purchased from Takara Biomedicals (Otsu, Japan). Murine kidneys (MRL/MpJ-+/+) were purchased from Japan SLC Inc. (Hamamatsu, Japan).

### Sample preparation

Proteins from murine kidneys were solubilized in lysis buffer (7 M urea, 2 M thiourea, 2% CHAPS, 30 mM Tris-HCl) by vor-

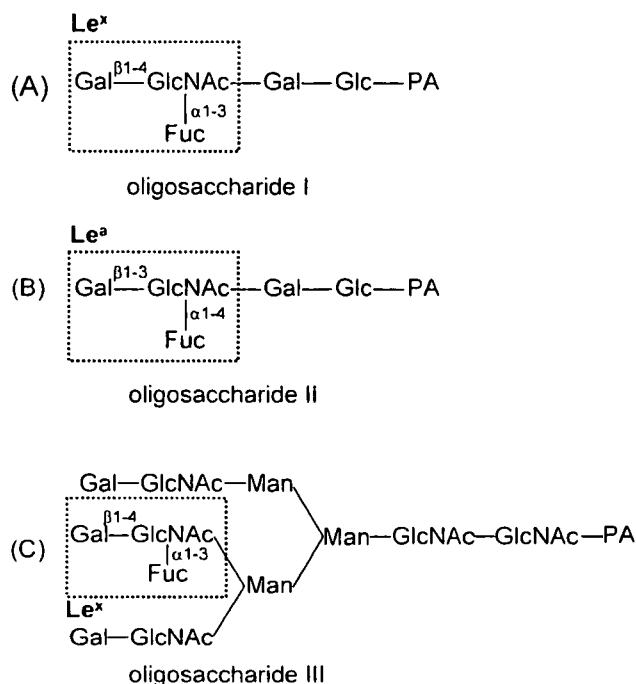


**Figure 2.** Structures of model oligosaccharides used in this study: (A) PA-labeled Le<sup>x</sup>-pentasaccharide (oligosaccharide I); (B) PA-labeled Le<sup>a</sup>-pentasaccharide (oligosaccharide II); and (C) PA-labeled Le<sup>x</sup>-asialotriantennary complex type oligosaccharide (oligosaccharide III).

texting at room temperature. The proteins (100  $\mu$ g) were recovered by precipitation in cold acetone, and then treated with 10 units of PNGase F in 500  $\mu$ L of 0.2 M phosphate buffer (pH 7.6) at 37°C for 48 h to release the *N*-linked oligosaccharides. Proteins were removed by precipitation in cold ethanol, and the supernatant containing oligosaccharides was evaporated and lyophilized. The dried oligosaccharides were labeled with PA according to a previous report.<sup>21</sup> The PA-labeled oligosaccharides were desalted with Envi-Carb C (Supelco Bellefonte, USA) and lyophilized.

### nanoESI-MS<sup>n</sup>

Experiments were performed using a Finnigan linear ion trap Fourier transform ion cyclotron resonance mass spectrometer (LTQ-FT, ThermoElectron, San Jose, CA, USA) equipped with a nanoESI source (AMR, Inc., Tokyo, Japan). ESI-MS<sup>n</sup> was carried out for Le<sup>x</sup>- and Le<sup>a</sup>-oligosaccharide standards at a concentration of 1 pmol/ $\mu$ L in 5 mM ammonium acetate and 10  $\mu$ M NaCl buffer (pH 9.6) containing 50% acetonitrile. The sample was analyzed at a flow rate of 2.0  $\mu$ L/min using a spray voltage of 2.0 kV in the positive ion mode. The capillary temperature was set to 200°C; collision energies were set to 20–30% for the MS<sup>n</sup> experiments; the maximum scan time was set to 50 ms. MS<sup>2</sup> and MS<sup>3</sup> were performed with an isolation width of 3.0 u (range of precursor ion  $\pm 1.5$ ).

### LC/MS<sup>n</sup>

LC was carried out using a MAGIC 2002 system (Michrom BioResources, Auburn, CA, USA) equipped with a GCC (Hypercarb column, 150  $\times$  0.2 mm, ThermoElectron). The

eluent were 5 mM ammonium acetate, pH 9.6, containing 2% acetonitrile (pump A) and 5 mM ammonium acetate, pH 9.6, containing 80% acetonitrile (pump B). PA-labeled *N*-linked oligosaccharides from murine kidney were eluted at a flow rate of 2  $\mu$ L/min with a gradient of 10–70% of pump B in 60 min. A solution of NaCl (10  $\mu$ M) was passed post-column at a flow rate of 2  $\mu$ L/min. The precursor ions detected by a full MS<sup>1</sup> scan (mass range at  $m/z$  750–2000) were followed by MS<sup>2</sup> scans of the most intense ions.

## RESULTS AND DISCUSSION

### MS<sup>n</sup> of Le<sup>x</sup>-pentaoligosaccharide

The model Le<sup>x</sup>-pentaoligosaccharide (oligosaccharide I) was analyzed by nanoESI-MS<sup>n</sup> with direct injection in the positive ion mode. Sodium chloride (NaCl) was deliberately added to the sample for the acceleration of the cross-ring cleavages according to previous reports.<sup>22–24</sup> The sodiated singly charged molecular ion, [M+Na]<sup>+</sup>, of oligosaccharide I was observed at  $m/z$  954.4 in the MS<sup>1</sup> spectrum (Fig. 3(A)). MS<sup>2</sup> of the sodiated molecular ion yielded [(M+Na)-Fuc]<sup>+</sup> at  $m/z$  808 as the most intense ion by the glycosidic bond cleavage between GlcNAc and Fuc residues (Fig. 3(B)). This indicates that the Fuc residue is easily dissociated by low-energy CID MS<sup>2</sup>. In addition to the defucosylated ions, we observed the sodiated ion at  $m/z$  534, corresponding to the Le<sup>x</sup> and Le<sup>a</sup> structure, [Gal(Fuc)GlcNAc+Na]<sup>+</sup>. The sodiated B<sub>2</sub> ion ( $m/z$  534) was subjected to a further product ion scan, and the sodiated ion at  $m/z$  388 corresponding to [GalGlcNAc+Na]<sup>+</sup> appeared in the MS<sup>3</sup> spectrum (Fig. 3(C)). The ion at  $m/z$  372, corresponding to [FucGlcNAc+Na]<sup>+</sup>, which proves the attachment of Fuc to GlcNAc, was also detected. Then, MS<sup>4</sup>

of the sodiated Y<sub>3 $\alpha$</sub>  ion ( $m/z$  388) yielded a sodiated cross-ring fragment ion at  $m/z$  259, corresponding to the sodiated <sup>3,5</sup>A<sub>2</sub> ion, which proves the linkage of the Gal residue at position C-4 on GlcNAc, with some neutral losses: 60 Da (<sup>0,4</sup>A<sub>2</sub>, <sup>0,4</sup>X<sub>4 $\beta$</sub> , <sup>1,3</sup>X<sub>4 $\beta$</sub>  and <sup>2,4</sup>X<sub>4 $\beta$</sub> ) and 90 Da (<sup>0,3</sup>X<sub>4 $\beta$</sub>  and <sup>1,4</sup>X<sub>4 $\beta$</sub> ) (Fig. 3(D)).

### MS<sup>n</sup> of Le<sup>a</sup>-pentaoligosaccharide

The Le<sup>a</sup>-pentaoligosaccharide (oligosaccharide II) was subjected to nanoESI-MS<sup>n</sup> in a similar manner. The [M+Na]<sup>+</sup> of oligosaccharide II was observed at  $m/z$  954.4 in the MS<sup>1</sup> spectrum (Fig. 4(A)). MS<sup>2</sup> of the [M+Na]<sup>+</sup> at  $m/z$  954 yielded the sodiated ion at  $m/z$  534, corresponding to [Gal(Fuc)GlcNAc+Na]<sup>+</sup> (Fig. 4(B)). MS<sup>3</sup> of the sodiated B<sub>2</sub> ion ( $m/z$  534) yielded the sodiated Y<sub>3 $\alpha$</sub>  and Y<sub>3 $\beta$</sub>  ions at  $m/z$  372 and 388, respectively (Fig. 4(C)). MS<sup>4</sup> of the sodiated Y<sub>3 $\beta$</sub>  ion at  $m/z$  388 yielded some cross-ring fragment ions at  $m/z$  208, 268, 298 and 328, corresponding to neutral losses: 60 Da (<sup>0,4</sup>A<sub>2</sub>, <sup>0,4</sup>X<sub>4 $\beta$</sub> , <sup>1,3</sup>X<sub>4 $\beta$</sub>  and <sup>2,4</sup>X<sub>4 $\beta$</sub> ) and 90 Da (<sup>0,3</sup>A<sub>2</sub>, <sup>0,3</sup>X<sub>4 $\beta$</sub>  and <sup>1,4</sup>X<sub>4 $\beta$</sub> ) (Fig. 4(D)). <sup>3,5</sup>A<sub>2</sub> at  $m/z$  259, which arose from oligosaccharide I, was not detected by MS<sup>4</sup> of Le<sup>a</sup>.

These results suggest that the Le<sup>x</sup> structure can be identified by the <sup>3,5</sup>A<sub>2</sub> ion at  $m/z$  259 generated by MS<sup>4</sup> of [GalGlcNAc+Na]<sup>+</sup> at  $m/z$  388, which arose from MS<sup>3</sup> [Gal(Fuc)GlcNAc+Na]<sup>+</sup> at  $m/z$  534 (Fig. 5).

### MS<sup>n</sup> of Le<sup>x</sup>-asialotriantennary oligosaccharide

Using a Le<sup>x</sup>-oligosaccharide with a more complicated branching structure, we confirmed the practicability of MS<sup>3</sup> of the ion at  $m/z$  534 followed by MS<sup>4</sup> of the ion at  $m/z$  388 for the detection of the Le<sup>x</sup>-diagnostic ion at  $m/z$  259.

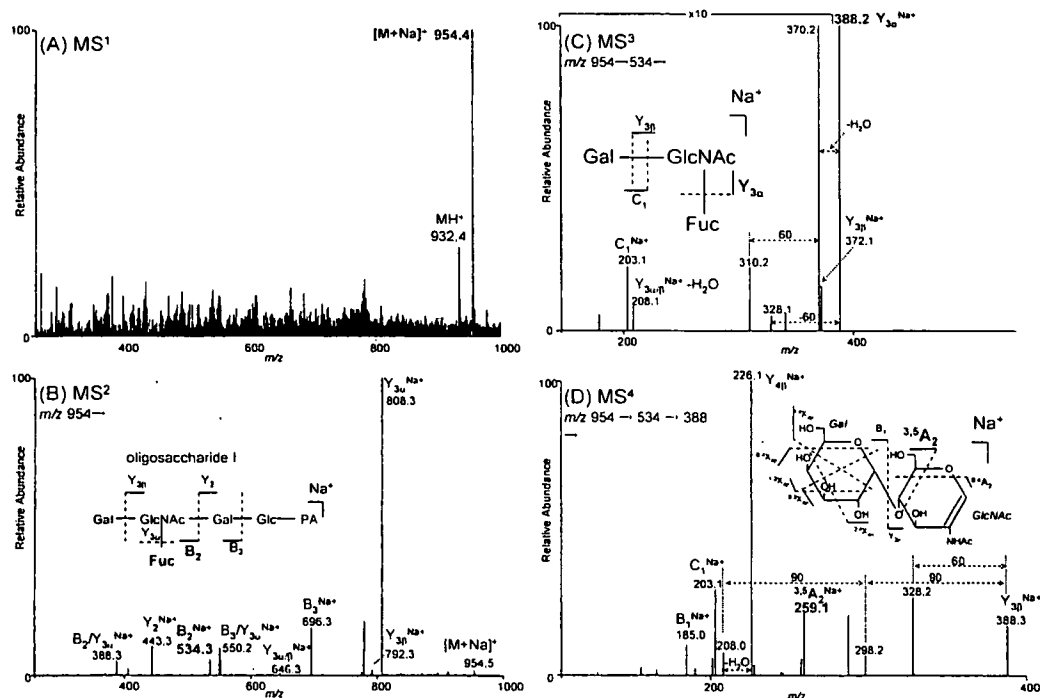


**Figure 3.** MS<sup>1–4</sup> spectra of oligosaccharide I by ESI-MS<sup>n</sup>: (A) MS<sup>1</sup> spectrum; (B) MS<sup>2</sup> spectrum of [M+Na]<sup>+</sup> at  $m/z$  954.4; (C) MS<sup>3</sup> spectrum of [Gal(Fuc)GlcNAc+Na]<sup>+</sup> at  $m/z$  534.3 detected in MS<sup>2</sup>; and (D) MS<sup>4</sup> spectrum of [GalGlcNAc+Na]<sup>+</sup> at  $m/z$  388.2 detected in MS<sup>3</sup>.